THEORY & BIO-SYSTEMS

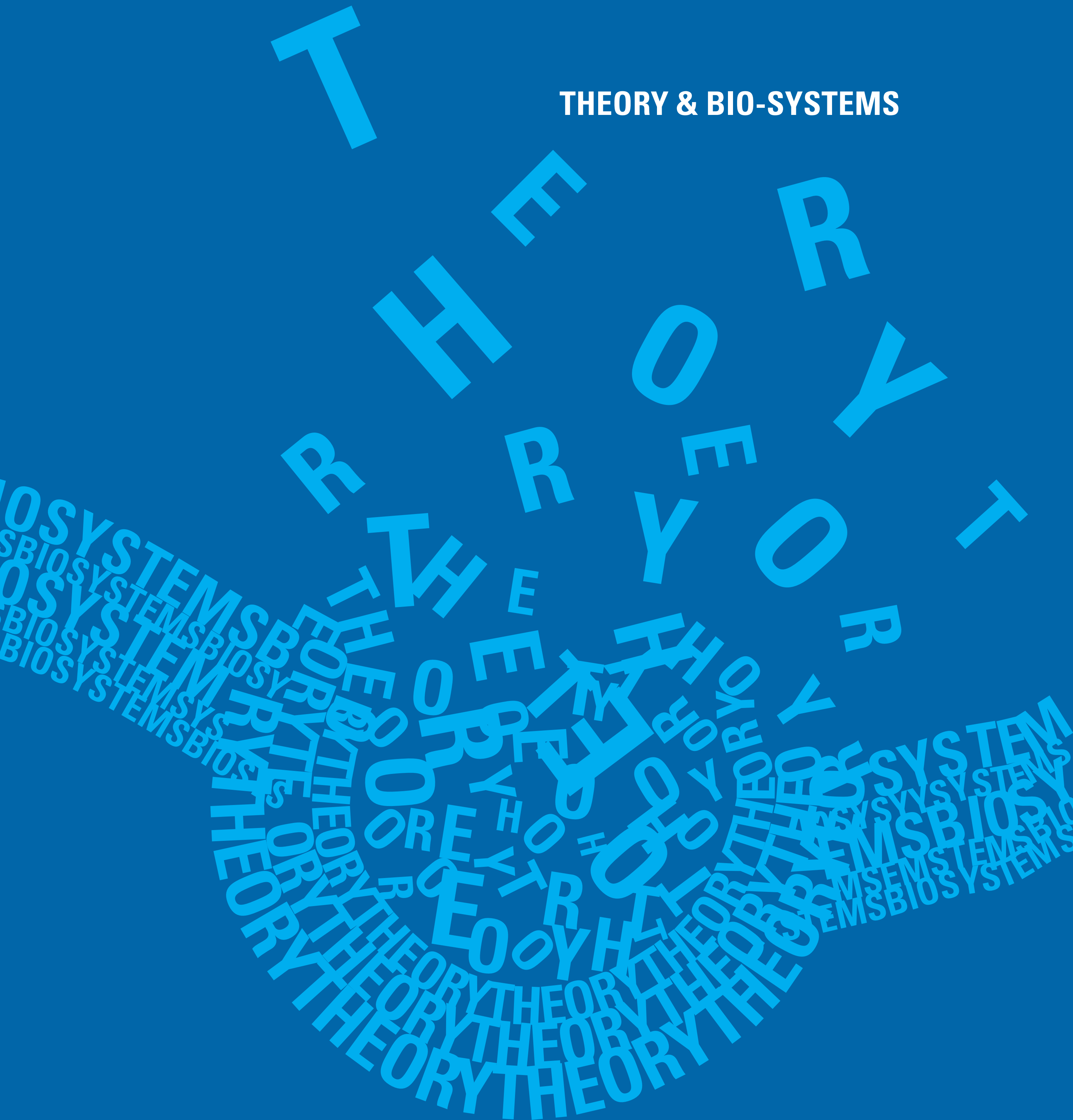

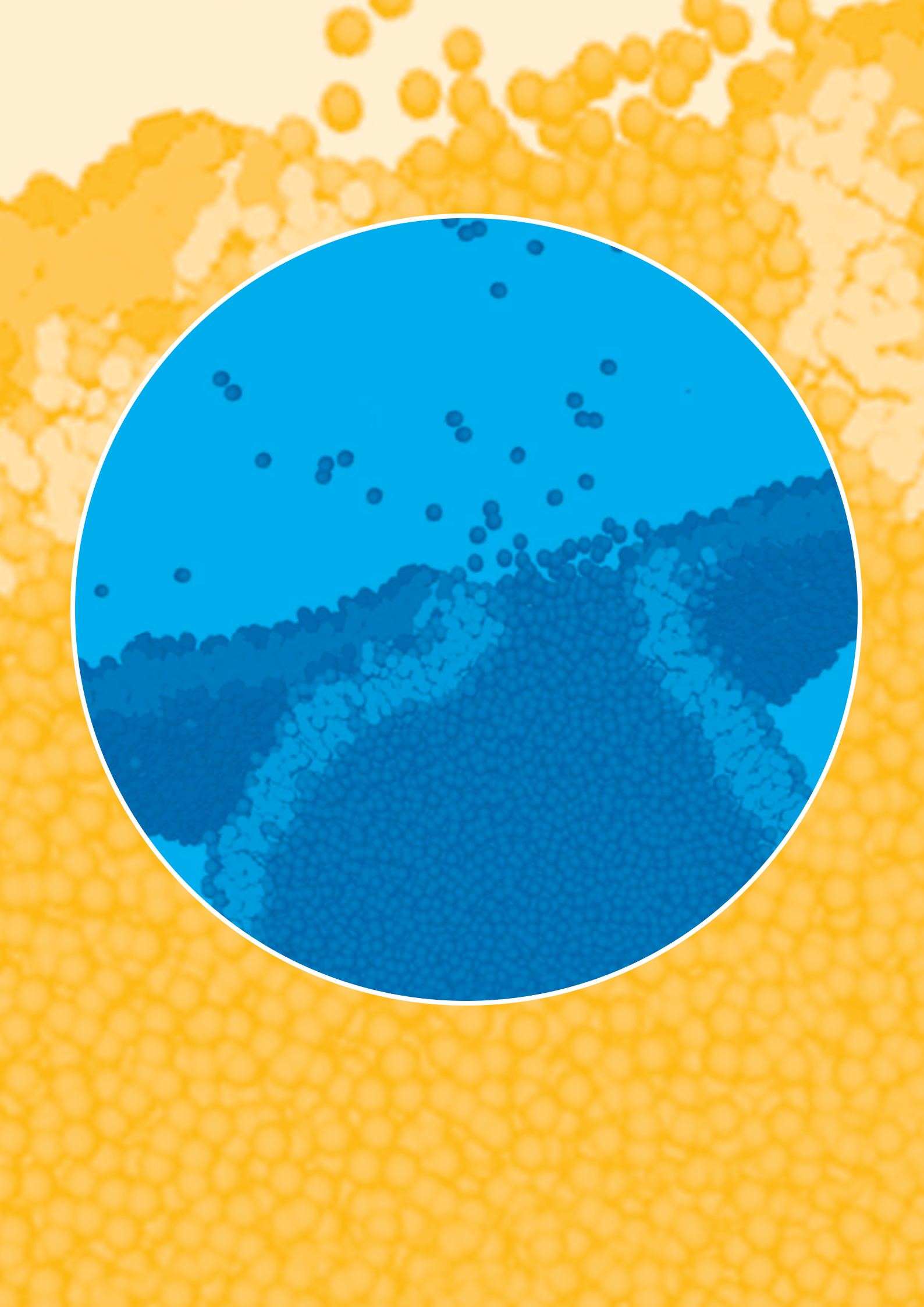

Research in the Department of Theory & Bio-Systems

So einfach wie möglich, aber nicht einfacher
Albert Einstein

The researchers and doctoral students of the Department of Theory and Bio-Systems form one experimental and six theoretical research teams. Each of these teams consists of the team leader and several students. The team leaders are:

- *Rumiana Dimova* (experiment, membranes and vesicles).
- *Thomas Gruhn* (theory, membranes and vesicles);
- *Jan Kierfeld* (theory, polymers and filaments);
- *Stefan Klumpp* (theory, transport by molecular motors; until 2005);
- *Volker Knecht* (theory; proteins and membranes; since 2006).
- *Christian Seidel* (theory, polymers and polyelectrolytes);
- *Julian Shillcock* (theory, supramolecular modelling; until 2005);
- *Thomas Weikl* (theory, proteins and membranes).

The Theory and Bio-Systems Department is responsible for and coordinates the International Max Planck Research School on "Biomimetic Systems", the European Early Stage Training Network about the same topic, in which three departments of the MPI participate, and the European Research Network on "Active Biomimetic Systems". The management of these networks is done by *Angelo Valleriani*.

In the following three subsections, the research within the Theory and Bio-Systems Department is described in terms of the underlying systems which exhibit a hierarchy of structural levels, the intriguing phenomena found in these systems, and the methods used to study them.

Systems

Our research is focused on bio-systems, which represents an abbreviation for "biomimetic and biological systems". If one looks at these systems bottom-up, i.e., from small to large length scales, one encounters a hierarchy of such systems including

- polymers and proteins,
- molecular motors,
- rods and filaments,
- membranes and vesicles, and
- networks in bio-systems.

When these systems are approached top-down, i.e., from larger to smaller scales, one encounters the problem of restricted geometries or confining walls and interfaces. In general, interfaces may be used to suspend and organize smaller bio-systems in order to make them accessible to systematic studies.

Phenomena

During the last two years, specific phenomena addressed in the area of polymers and proteins included the conformation of peptides at interfaces, the process of protein folding, and dense brushes of polyelectrolytes. As far as motor proteins or molecular motors are concerned, we studied the chemomechanical coupling of single motors and the cooperative transport by several such motors, see **Fig. 1**.

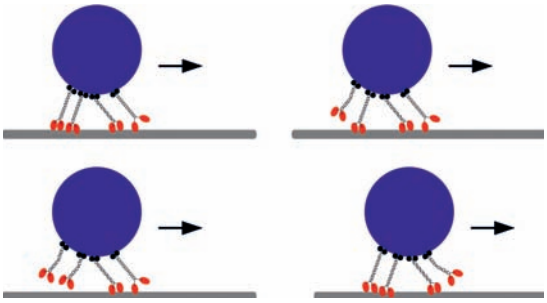

Fig. 1: Cooperative transport of cargo by several molecular motors

The cooperative behavior of rods and filaments provides many unusual phenomena such as the active polymerization of filaments, the ordering of filaments on substrate surfaces covered with immobilized molecular motors, see **Fig. 2**, and ordered mesophases of rods with adhesive endgroups.

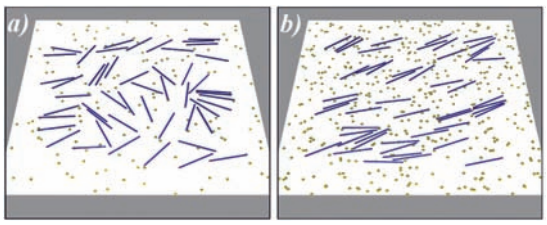

Fig. 2: (a) Disordered and (b) Ordered nematic states of rod-like filaments (blue) on a substrate surface with immobilized molecular motors (yellow spots). The transition from (a) to (b) is induced by an increase in the motor density.

In the research field of membranes and vesicles, we have improved our theoretical models for membrane fusion and membrane adhesion. A timely topic is the adhesion of membranes via specific molecular bonds, see **Fig.3**. In addition, the direct imaging of intramembrane domains and vesicle fusion has been further developed, see **Fig. 4**.

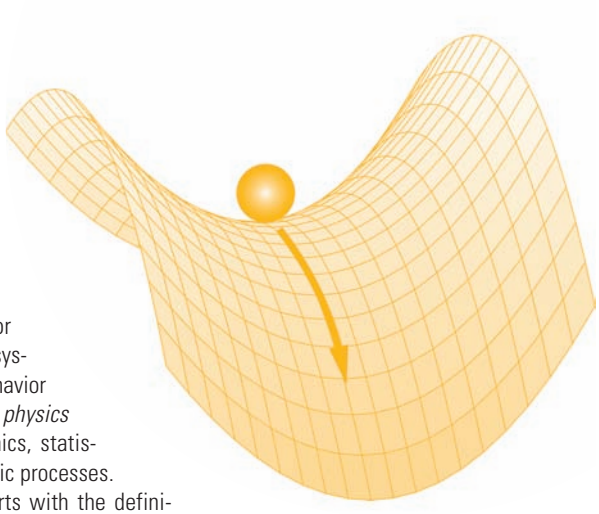

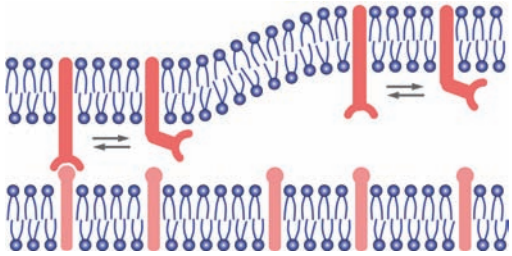

Fig. 3: Adhesion of two membranes via active receptors or stickers that can attain both an adhesive and a non-adhesive state.

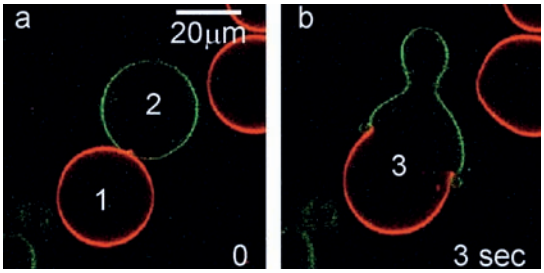

Fig. 4: Fusion of giant vesicles as observed by fluorescence microscopy. The two colors (red and green) correspond to two different membrane compositions that form stable domains after the fusion process has been completed.

Bio-systems are quite complex and exhibit many levels of self-organization. One rather general framework for these systems is provided by network models. During the last two years, we have worked on networks of motor cycles, activity pattern on scale-free networks, and network models for biological evolution.

All systems and phenomena that have been mentioned in this overview will be covered in more detail on the following pages.

Methods

The conceptual framework for the understanding of these systems and their cooperative behavior is provided by *statistical physics* which includes thermodynamics, statistical mechanics, and stochastic processes.

Our theoretical work starts with the definition of a certain model which (i) is amenable to systematic theoretical analysis and (ii) captures the essential features of the real system and its behavior. New models which have been introduced in our department include: semi-flexible harmonic chains for filaments; coarse-grained molecular models for bilayer membranes; lattice models for membranes with adhesion molecules; geometric models for membranes with lateral domains; lattice models for transport by molecular motors; Markov models for cooperative motor transport as well as network models for motor cycles.

These theoretical models are then studied using the analytical tools of theoretical physics and a variety of numerical algorithms. The analytical tools include dimensional analysis, scaling arguments, molecular field or self-consistent theories, perturbation theories, and field-theoretic methods such as renormalization. The numerical methods include the application of mathematical software packages such as Mathematica or Maple as well as special algorithms such as, e.g., the Surface Evolver for the calculation of constant mean curvature surfaces.

Several types of computer simulations are applied and further developed: Molecular Dynamics, Dissipative Particle Dynamics, and Monte Carlo methods. Molecular Dynamics is used for particle based models of supra-molecular assemblies; Dissipative Particle Dynamics, which is a relatively new simulation algorithm, is useful in order to extend the Molecular Dynamics Studies towards larger systems and longer time scales; Monte Carlo methods are used in order to simulate even larger mesoscopic systems such as filaments and membranes up to a linear size of hundreds of nanometers.

The experimental work is carried out in our membrane lab which is equipped with calorimetry, optical microscopy, micropipettes, and optical tweezers. This lab is also responsible for the advanced confocal microscope that is available to all four departments of the MPI.

Additional information about research in the Theory Department is available at *www.mpikg.mpg.de/th/*

Reinhard Lipowsky
Director of the Department of Theory & Bio-Systems

Peptide Folding, Aggregation, and Adsorption at Interfaces

Volker Knecht 06.01.1970
1996: Diploma in physics (University of Kaiserslautern)
Thesis: Computer based renormalization group study of the two-dimensional XY model
1997: Software trainee (TECMATH GmbH, Kaiserslautern)
1998-1999: Software engineer (LMS Durability Technologies GmbH, Kaiserslautern)
2003: PhD, Physics (MPI of biophysical chemistry, Göttingen)
Thesis: Mechanical coupling via the membrane fusion SNARE protein syntaxin 1A: a molecular dynamics study
2003-2005: Postdoc (University of Groningen, the Netherlands)
2005-2006: Postdoc (MPI of Colloids and Interfaces, Potsdam)
Since 2006: Group Leader (MPI of Colloids and Interfaces, Potsdam)

A number of neurodegenerative diseases such as Alzheimer's or Parkinson's are related to the precipitation of protein into β-sheet rich amyloid fibrils. The transformation of a protein from the functional soluble state to the pathogenic fibril state is believed to be initiated by a misfolding of the protein and the formation of small oligomers. Interfaces can promote or inhibit fibril formation depending on the amino acid sequence of a peptide and the molecular structure of the interface. To study the early steps of fibril formation in atomic detail experimentally is difficult due to the tendency of misfolded proteins to aggregate and the short lifetimes of small oligomers. Computer simulations therefore provide an indispensable tool to study these processes.

We employ molecular dynamics simulations to study fibril forming peptides in solution and at interfaces as model systems. In our simulations, peptide(s) and solvent environment are described in atomic detail. Atoms are modeled as classical point masses whose interaction is described using a semi-empirical force field. The simulations provide a high spatial and temporal resolution of biomolecular processes. However, due to their computational expense such simulations suffer from a notorious sampling problem. Therefore, experimental data are important bench-marks for the simulations. In a collaboration with the group of Gerald Brezesinski from the interfaces department, we have studied the fibrillogenic peptide B18, a fragment of the sea urchin fertilization protein Bindin and corresponding to resides 103-120 of the parent protein **[1-3]**.

In water, B18 tends to form β-strand-loop-β-strand conformations (see Fig. 1(a) *middle*). β-sheets are mainly formed by hydrophobic residues (*yellow*). In the initial steps of the adsorption at a water/vapor interface, α-helical and turn conformations are induced in the C-terminal segment which is partially hydrophilic (see **Fig. 1(a)** right) **[1]**. Upon adsorption to a (negatively charged) DPPG monolayer, B18 becomes somewhat more disordered. The effect of the environment on the peptide structure is in agreement with data from circular dichroism (CD) and infrared spectroscopy **[2]**. For the first time, we have studied the formation of partially ordered dimers of strand-loop-strand forming peptides in explicit solvent (see **Fig. 1(b)**) **[3]**. Whereas previous simulations using implicit solvation models predicted planar aggregates, we observe highly twisted β-sheet structures, indicating the twist to be (partially) a specific solvent effect.

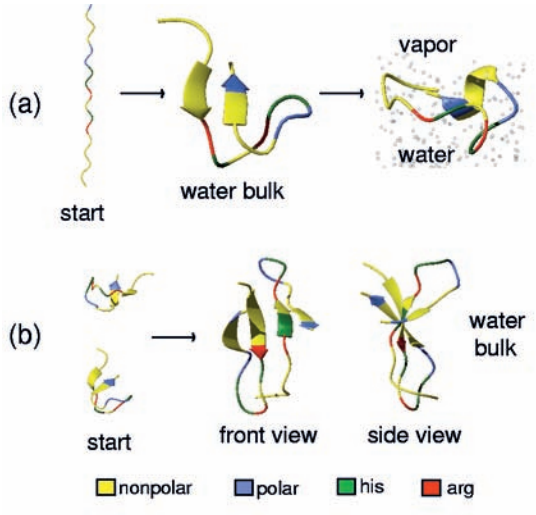

Fig. 1: Folding and aggregation of B18 peptide in different environments in molecular dynamics simulations. (a) In water, B18 tends to adopt β-strand-loop-β-strand structures (middle). Adsorption to a water/vapor interface induces α-helical conformations (right). (b) In water bulk, partially ordered β-sheet rich dimers can form on a nanosecond timescale. The peptide backbone is shown in ribbon representation, the amino acid sequence is color-coded.

In water, pre-formed α-helical conformations are partially kinetically trapped on the nanosecond timescale of our simulations at room temperature, but convert into β-sheet structures at elevated temperature as shown in **Fig. 2**. The transition is initiated by a quick hydrophobic collapse (see **Fig. 2(c,d)**). α-helical conformations dissolve into turn and coil conformations (see **Fig. 2(a,b)**) and the number of main chain hydrogen bonds decreases (see **Fig. 2(e)**). Upon formation of β-sheets (see **Fig. 2(b)**), the peptide becomes more extended again (see **Fig. 2(c)**).

A water/vapor interface stabilizes α-helical conformations in agreement with infrared data. This finding allowed the usage of a coarse grain model in which the peptide was described as a rigid helix and facilitated to study the lateral organization of multiple B18 peptide and DPPC molecules in the interface. As shown in **Fig. 3**, B18 and DPPC demix in the interface and B18 accumulates in the three-phase boundary between water, lipid, and vapor phase. At the equilibrium lateral pressure (known from experiment), the interface is fully covered by peptide and lipid molecules which remain demixed (see **Fig. 3**, right). The demixing of B18 and DPPC molecules in a water/vapor interface explains the experimental observation that adsorption of B18 to a DPPC monolayer in the liquid-expanded gas coexistence region does not change the structure of the DPPC monolayer **[1]**.

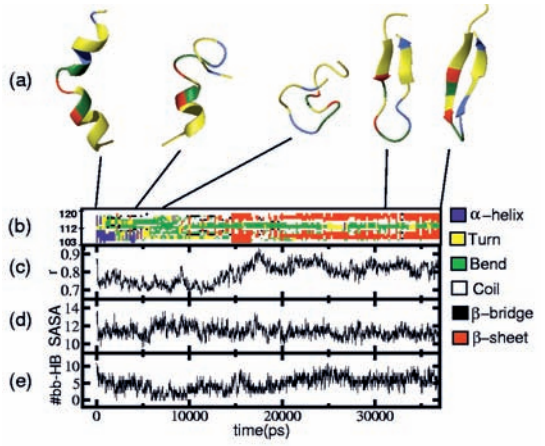

Fig. 2: α-β transition of B18 in water at elevated temperature involving a compact coil intermediate. (a) selected configurations. (b) Time evolution of the secondary structure obtained from an analysis of backbone hydrogen bonds. Here the vertical coordinate represents the residue number which is plotted against time, and the secondary structure is color-coded. (c-e) Time evolutions of (c) radius of gyration (measure of compactness of the peptide), (d) hydrophobic solvent-accessible surface area (measure of the exposure of nonpolar groups to the solvent), and (e) number of peptide main chain hydrogen bonds.

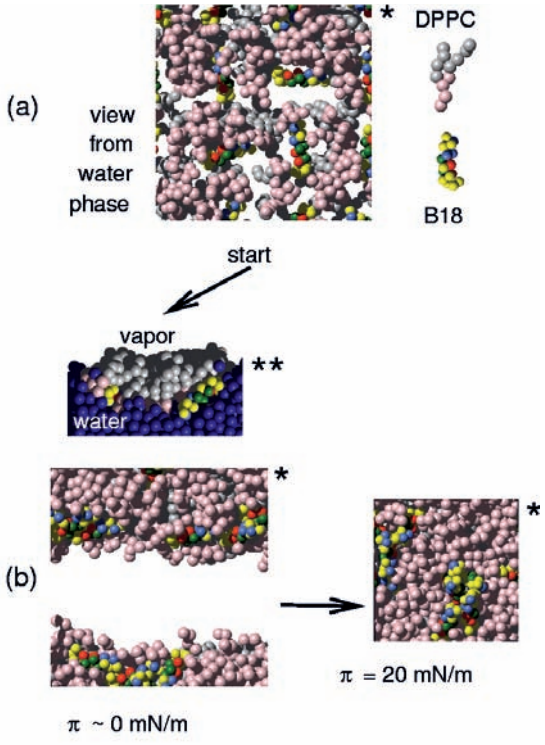

Fig. 3: Demixing of B18 peptide and DPPC lipid molecules in a water/vapor interface in simulations using a coarse grain model. (a) As initial configuration, a random distribution of molecules in the interface was used. (b, left) During a simulation peptide and lipid molecules demix spontaneously. Peptides accumulate in the three phase boundary between water, lipid, and vapor. (b, right) At the equilibrium lateral pressure (known from experiment), the interface is fully covered by peptide and lipid molecules which remain demixed. Views of configurations normal to the interface towards the vapor phase (*) or parallel to the interface (**) are shown.

Future Work

Ongoing work is focused on (i) sequence effects on the folding and aggregation of amyloid forming peptides, (ii) membrane fusion, and (iii) electrokinetic phenomena. PhD student Madeleine Kittner who started at the beginning of January 2007 will work on peptides. Another member starting in the coming months will work on membrane fusion. A PhD student starting in February 2007 will work on a new project, (iv) modeling of molecular motors with atomic resolution. Besides these molecular dynamics studies, (v) a mesoscopic study of pore formation in membranes is carried out by the postdoc Josep Pamies.

V. Knecht, M. Kittner, J. Pamies
vknecht@mpikg.mpg.de

References:

[1] V. Knecht, H. Möhwald, and R. Lipowsky, Conformational diversity of the fibrillogenic fusion peptide B18 in different environments from molecular dynamics simulations, J. Phys. Chem. B, **111**, 4161-4170, 2007

[2] E. Maltseva, Model membrane interactions with ions and peptides at the air/water interface, Ph.D. thesis, Universität Potsdam (2005).

[3] V. Knecht and R. Lipowsky, Dimerization of the fibrillogenic peptide B18 in water in atomic detail, in preparation.

Protein Folding

Thomas Weikl 01.04.1970
1996: Diploma, Physics
(Freie Universität Berlin)
Thesis: Interactions of rigid membrane inclusions
1999: PhD, Physics
(Max Planck Institute of Colloids and Interfaces, Potsdam)
Thesis: Adhesion of multicomponent membranes
2000-2002: Postdoc
(University of California, San Francisco)
Since 2002: Group Leader
(Max Planck Institute of Colloids and Interfaces, Potsdam)

Proteins are chain molecules built from amino acids. The precise sequence of the twenty different types of amino acids in a protein chain defines into which structure a protein folds, and the three-dimensional structure in turn specifies the biological function of a protein. The reliable folding of proteins is a prerequisite for their robust function. Misfolding can lead to protein aggregates that cause severe diseases, such as Alzheimer's, Parkinson's, or the variant Creutzfeldt-Jakob disease.

To understand protein folding, researchers have long focused on metastable folding intermediates, which were thought to guide the unfolded protein chain into its folded structure. But about a decade ago, small proteins were discovered that fold without any detectable intermediates (see **Fig. 1**). This astonishingly direct folding from the unfolded state into the folded state has been termed 'two-state folding'. In the past years, the majority of small single-domain proteins have been identified as 'two-state folders'.

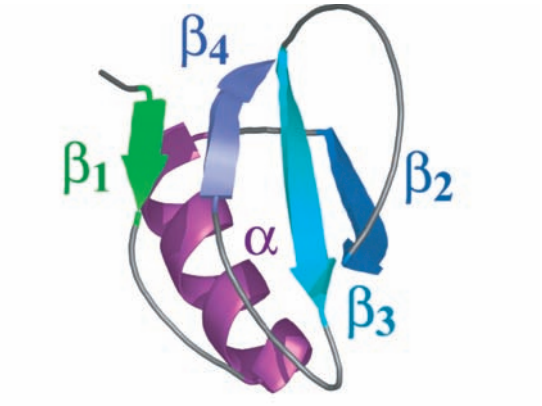

Fig. 1: The small protein CI2 is two-state folder, i.e. a protein that does not exhibit metastable intermediates states between the unfolded and the folded state. The structure of CI2 consists of an α-helix packed against a four-stranded β-sheet.

The characteristic event of two-state folding is the crossing of a barrier between the unfolded and the folded state (see **Fig. 2**). This folding barrier is thought to consist of a large number of extremely short-lived transition state structures. Each of these structures is partially folded and will either complete the folding process or will unfold again, with equal probability. In this respect, transition state structures are similar to a ball on a saddle point that has the same probability 1/2 of rolling to either side of the saddle (see **Fig. 3**).

Since transition state structures are highly instable, they cannot be observed directly. To explore two-state folding, experimentalists instead create mutants of a protein. The mutants typically differ from the original protein, the wild type, just in a single amino acid. The majority of these mutants still fold into the same structure. But the mutations may slightly change the transition state barrier and, thus, the folding time, the time an unfolded protein chain on average needs to cross the folding barrier (see **Fig. 4**).

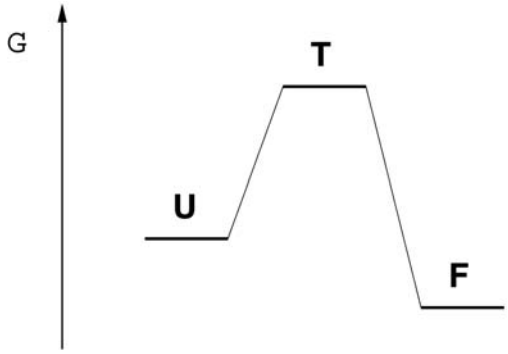

Fig. 2: The folding dynamics of two-state proteins is dominated by the transition state T between the unfolded state U and the folded state F. The transition state is a barrier in the free energy G. The folding time of a protein depends on the height of this free energy barrier.

The central question is how to reconstruct the transition state from the observed changes in the folding times. Such a reconstruction clearly requires experimental data on a large number of mutants. In the traditional interpretation, the structural information is extracted for each mutation independent of the other mutations. If a mutation does not change the folding time, then the mutated amino acid traditionally is interpreted to be still unstructured in the transition state. In contrast, if a mutation changes the folding time, the mutated amino acid is interpreted to be partially or fully structured in the transition state, depending on the magnitude of the change.

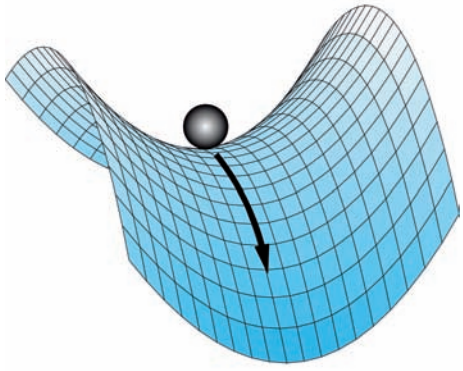

Fig. 3: A ball on a saddle point has the probability 1/2 of rolling to either side of the saddle. The transition state structures that make up the transition state correspond to such saddle points.

However, this traditional interpretation often is not consistent. For example, twenty single-residue mutations in the α-helix of the protein Chymotrypsin Inhibitor 2 (CI2) have very different effects on the folding time. Naively interpreted, these differences seem to indicate that some of the helical residues are unstructured in the transition state, while other residues, often direct neighbors, are highly structured. This

naive interpretation is in contradiction with the fact that the folding of helices is cooperative and can only occur if several consecutive helical turns are structured, stabilizing each other.

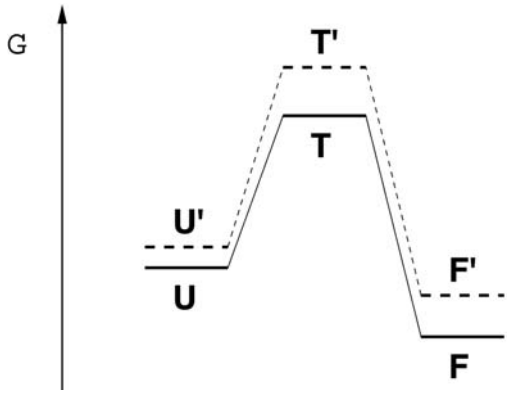

Fig. 4: Mutations of a protein shift the free energy of the unfolded state U, folded state F, and transition state T. The shift of the free energy barrier can be determined from experimentally measured folding times for the wildtype and the mutant proteins. Theoretical modelling of the experimental data leads to structural information on the transition state.

We have suggested a novel interpretation of the mutational data **[1,2]**. Instead of considering each mutation on its own, the new interpretation collectively considers all mutations within a cooperative substructure, such as a helix. In case of the α-helix of the protein CI2, this leads to a structurally consistent picture in which the helix is fully formed in the transition state, but has not yet formed significant interactions with the β-sheet. Also for other helices, we obtain a consistent structural interpretation of the mutational data **[2]**.

Currently, we focus on the construction of complete transition states from mutational data. An important step is to identify the cooperative subunits of a protein, which requires molecular modeling. To identify cooperative subunits of the protein CI2 (see **Fig. 1**), we have studied a large number of Molecular Dynamics unfolding trajectories **[3]**. On each unfolding trajectory, we determine the opening times of all amino-acid contacts of the folded structure. We find that the cooperative subunits of this protein correspond to four structural elements: the α-helix, and the three β-strand pairings $\beta_2\beta_3$, $\beta_3\beta_4$ and $\beta_1\beta_4$. We obtain high correlations between the opening times of contacts of the same structural elements, and observe lower correlations between contacts of different structural elements (see **Fig. 4**).

In addition, we have developed concepts that help to understand why some structural elements are central for the folding dynamics. The transition-state free-energy barrier of a protein is largely entropic. An important contribution is the loop-closure entropy that is lost when the protein chain forms contacts between amino acids during folding. This loss in loop-closure entropy depends on the sequence in which the contacts are formed **[4,5]**. Using graph-theoretical concepts to estimate loop lengths in a partially folded protein chain, we have identified contact sequences, or folding routes, with low entropy loss **[4]**. On these routes, some structural elements form early and effectively reduce the loop lengths of other structural elements, which results in a smaller entropy loss for forming the structural elements.

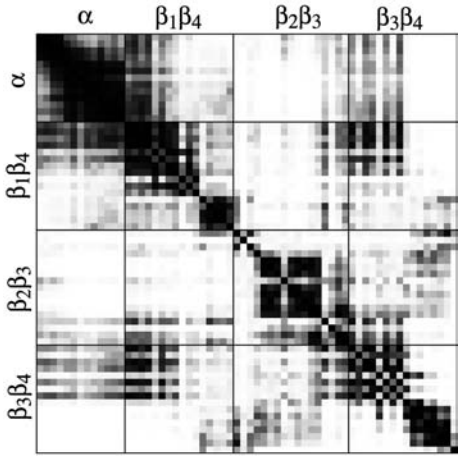

Fig. 5: Correlations between amino-acid contacts of the protein CI2 measured o a large number of Molecular Dynamics unfolding trajectories. The contacts are ordered according to the structural elements they belong to. Dark gray colors correspond to high correlations between pairs of contacts, light grey colors to low correlations. The dark colors along the diagonal of the correlation matrix indicate high correlations between contacts of the same structural element. The dark colors in the upper left square of the matrix, for example, indicate that the amino-acid contacts of the α-helix unfold highly cooperatively.

T. Weikl, C. Merlo, L. Reich
thomas.weikl@mpikg.mpg.de

References:

[1] Merlo, C., Dill, K.A., and Weikl, T.R.: Φ-values in protein folding kinetics have energetic and structural components. Proc. Natl. Acad. Sci. USA **102**, 10171-10175 (2005).

[2] Weikl, T.R., and Dill, K.A.: Transition states in protein folding kinetics: The structural interpretation of Φ-values. J. Mol. Biol. **365**, 1578-1586 (2007).

[3] Reich, L., and Weikl, T.R.: Substructural cooperativity and parallel versus sequential events during protein unfolding. Proteins **63**, 1052-1058 (2006).

[4] Weikl, T.R.: Loop-closure events during protein folding: Rationalizing the shape of Φ-value distributions. Proteins **60**, 701-711 (2005).

[5] Dixit, P.D., and Weikl, T.R.: A simple measure of native-state topology and chain connectivity predicts the folding rates of two-state proteins with and without crosslinks. Proteins **64**, 193-197 (2006).

Polymer Brushes

Christian Seidel 07.02.1949
1972: Diploma, Physics (Technical University Dresden) Thesis: Calculation of angular distribution and polarization of nucleon scattering close to resonance energies
1978: Dr. rer. nat., Polymer Physics (Institute for Polymer Chemistry, Teltow) Thesis: On the calculation of the phonon dispersion of solid polymers, application to polyvinylidenfluoride
1979-83: Research Scientist (Joffe Physico-Technical Institute, Leningrad)
1983-89: Research Scientist (Institute for Polymer Chemistry, Teltow)
1985: Dr. sc. nat., Solid State Theory (Institute for Polymer Chemistry, Teltow) Thesis: Ground states and critical temperatures in quasi-one-dimensional systems
1989-91: Group Leader (Institute for Polymer Chemistry, Teltow)
Since 1992: Group Leader (Max Planck Institute of Colloids and Interfaces, Potsdam)
1994: Habilitation, Theoretical Chemistry (Technical University, Berlin)

Polymer brushes consist of chains densely end-grafted to a surface. Compared to polymers in solution, a new length scale is present in grafted systems: the distance between grafting points $d = A^{1/2}$ with A being the average area per polymer at the interface. When the grafting density $\rho_a = 1/A$ is high, nearby chains repel each other, forcing the polymer to stretch out away from the grafting plane. Such systems have important technological applications which range from colloidal stabilization and lubrication to nanoparticle formation at the polymer brush/air interface. In biological sciences, there is a growing interest in polymer brushes as model systems of cell surfaces.

If the grafted polymer is a polyelectrolyte (PEL), i.e., contains monomers which have the ability to dissociate charges in polar solvents such as, e.g. water, the behavior of the brush is basically governed by the osmotic pressure of free counterions. A strongly charged PEL brush is able to trap its own counterions generating a layer of high ionic strength. Therefore a surface coated with PELs is less sensitive to the salinity of the surrounding medium as a bare charged surface. Nevertheless varying salt concentration is an important parameter to tune the polyelectrolyte effect and to change the structure of PELs.

Polyelectrolyte Brushes with Additional Salt [1, 2]

According to Pincus **[3]** the PEL brush shrinks with increasing salt concentration, but only as a relatively weak power law $c_s^{-1/3}$. There is some experimental and theoretical work that confirms this prediction, but there are other results that are in contradiction. The aim of our molecular dynamics (MD) simulation study was to clarify that question.

Fig.1a shows the brush height as a function of salt concentration where we plot $h(c_s)/h_{th}$ vs $bc_s/(\rho_a f^{1/2})$ with b being the monomer size and f the degree of dissociation. (In this study we use fully charged PELs, i.e., f = const = 1.) The brush height h_{th} is theoretically predicted to have the form $h_{th} = Nb\,(f + \sigma^2_{eff}\,\rho_a) / (1 + f)$ in the nonlinear osmotic regime without salt **[4]** with N being the chain length and σ_{eff} the effective polymer radius. Indeed all data points fall onto a universal scaling curve indicating again the validity of the nonlinear osmotic brush relation.

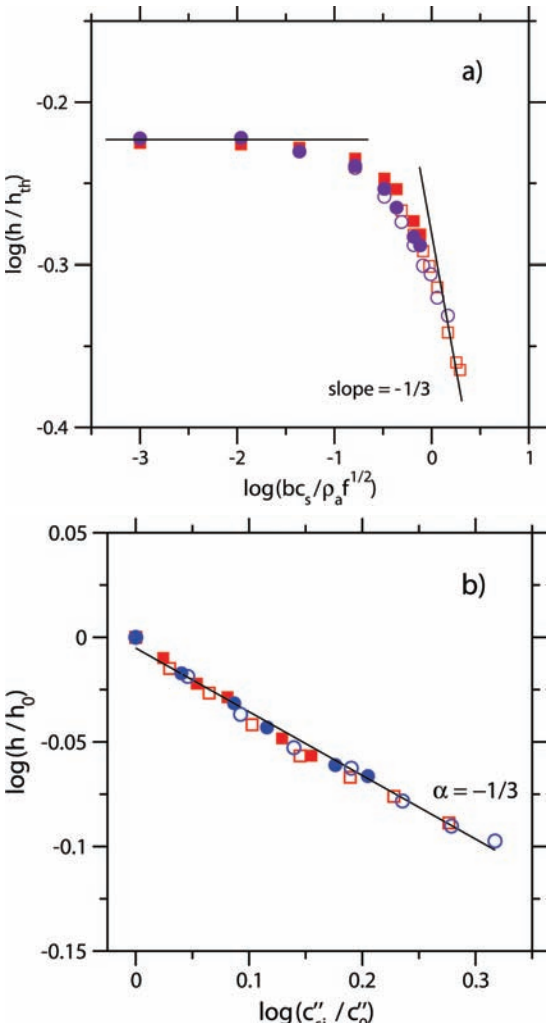

Fig. 1: Polyelectrolyte brushes with additional salt at grafting density 0.04 (circles) and 0.09 (squares). a) Brush height as a function of salt concentration, b) brush height as a function of total ion concentration.

For small c_s (i.e., $c_s << c_{ci}$ with c_{ci} being the counterion concentration), the influence of salt disappears. With growing c_s we obtain a broad cross over which merges at large salt concentration into the $c_s^{-1/3}$ power law predicted theoretically. However, the limit $c_s >> c_{ci}$ is hard to fulfill within the given numerical limitations. That is why we additionally study the brush height as a function of the total concentration of (free) ions inside the brush, i.e., taking into account counterions too. The corresponding plot is shown in **Fig. 1b** where we observe an almost perfect agreement with the scaling prediction.

Interacting Polyelectrolyte Brushes [2, 5]

PEL brushes attached to surfaces rubbing across an aqueous medium provide means of efficient lubrication. The interaction between two PEL brushes which are grafted to two apposing surfaces has recently received a lot of attention in experiments and simulations. Within the scaling approach **[3]** the disjoining pressure of two overlapping PEL brushes grafted to surfaces separated by a distance $2D$ is given by the counterion osmotic pressure $\Pi \sim k_B T f N \rho_a / D$. As the brushes are approaching two processes occur: interpenetration and compression.

Fig. 2 shows snapshots taken from simulations with varying distance between the two brushes. Note the strong exchange of counterions between the two brushes. At large separations the brush height remains almost constant. However, before overlapping at $D = h_{th}$ the chains begin to contract.

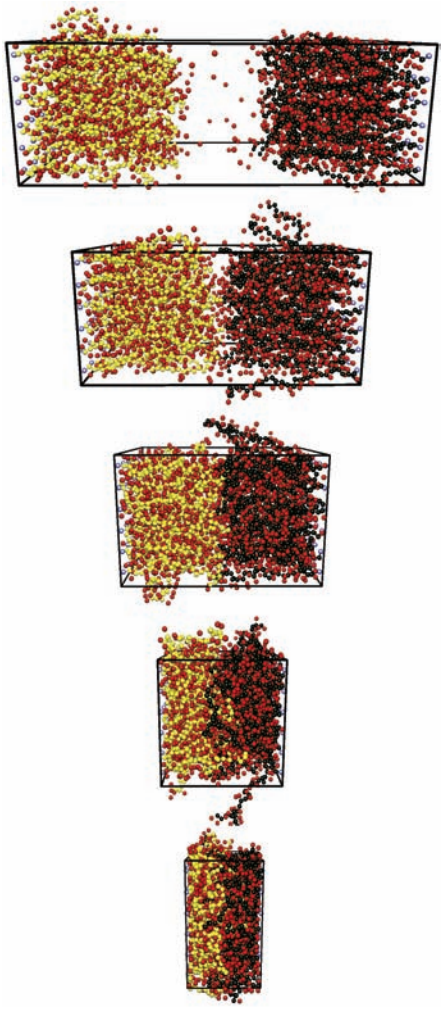

Fig. 2: Snapshots of two interacting polyelectrolyte brushes at decreasing separation D/h_{th} = 1.7, 1.2, 0.9, 0.6, and 0.3 from top to bottom. Monomers are colored yellow and dark green, respectively, counterions red.

In **Fig. 3** we plot the pressure as a function of separation. In fact, at $D > D^*$, the behavior of an ideal gas of counterions $\Pi \sim 1/D$ is reproduced. On the other hand, below D^* the pressure shows features expected in the excluded-volume-dominated regime. From our simulations, we find that the crossover occurs at $D^* \approx 1.4\ h_{th}$, i.e., before the two brushes strongly overlap. In the excluded-volume-dominated regime we observe a transition from good solvent behavior $\Pi \sim 1/D^2$ to θ behavior $\Pi \sim 1/D^3$ with increasing grafting density.

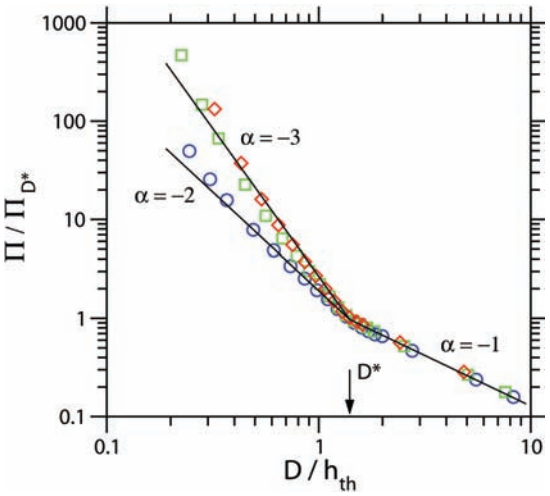

Fig. 3: Two interacting polyelectrolyte brushes. Pressure as a function of separation at grafting density 0.04 (circles), 0.09 (squares), 0.12 (diamonds).

DPD Simulation of Polymer Brushes [6]

The structure of (uncharged) polymer brushes was investigated by dissipative particle dynamics (DPD) simulations that include explicit solvent particles. With an appropriate choice of the DPD interaction parameters, we obtain good agreement with previous MD simulation results where the good solvent behavior has been modeled by an effective monomer-monomer potential. The relation between the Lennard-Jones length scale σ and the DPD scale r_c is found to be $r_c = 1.9\ \sigma$.

This study was implemented to benchmark DPD simulations of polymer brushes for subsequent large length scale simulations. DPD simulations to study nanoparticle aggregation inside a polymer brush are currently under progress.

C. Seidel, A. Kumar, S. Pal
seidel@mpikg.mpg.de

References:

[1] Kumar, N.A. and Seidel, C.: Polyelectrolyte Brushes with Added Salt. Macromol. **38**, 9341-9350 (2005).
[2] Kumar, N.A.: Molecular Dynamics Simulations of Polyelectrolyte Brushes. PhD Thesis, University of Potsdam (2006).
[3] Pincus, P.: Colloid Stabilization with Grafted Polyelectrolytes. Macromol. **24**, 2912-2919 (1991).
[4] Naji, A., Seidel, C. and Netz, R.R.: Theoretical Approaches to Neutral and Charged Polymer Brushes. Adv. Polym. Sci. **198**, 149-183 (2006).
[5] Kumar, N.A. and Seidel, C.: Interaction between Two Polyelectrolyte Brushes. Submitted to Phys. Rev. Lett.
[6] Pal, S. and Seidel, C.: DPD Simulations of Polymer Brushes. Macromol. Theory and Sim. **15**, 668-673 (2006).

Chemomechanical Coupling of Molecular Motors

Reinhard Lipowsky 11.11.1953
1978: Diploma, Physics,
Thesis with Heinz Horner on
turbulence (University of Heidelberg)
1982: PhD (Dr. rer. nat.), Physics
(University of Munich)
Thesis with Herbert Wagner
on surface phase transitions
1979-1984: Teaching Associate with
Herbert Wagner (University of Munich)
1984-1986: Research Associate with
Michael E. Fisher (Cornell University)
1986-1988: Research Associate with
Heiner Müller-Krumbhaar (FZ Jülich)
1987: Habilitation, Theoretical Physics
(University of Munich)
Thesis: Critical behavior of interfaces:
Wetting, surface melting and related
phenomena
1989-1990: Associate Professorship
(University of Munich)
1990-1993: Full Professorship
(University of Cologne), Director of
the Division "Theory II" (FZ Jülich)
Since Nov 1993: Director
(Max Planck Institute of Colloids
and Interfaces, Potsdam)

Living cells contain a large number of molecular motors: membrane pumps, stepping motors, growing filaments, and molecular assemblers such as polymerases and ribosomes. In many cases, these nanomachines are driven by the energy released from fuel molecules such as adenosine triphosphate (ATP). The coupling of the motor to these non-equilibrium reactions provides energy which is converted into conformational transformations of the motor and enables it to perform useful work.

Linear Stepping Motors with Two Motor Heads

The conversion of chemical energy into mechanical work is particularly striking for linear stepping motors such as kinesin, see **Fig. 1**, whose movements cover many length and time scales **[1]**. These motors have two heads, by which they bind to and walk along actin filaments and microtubules. In their bound states, they undergo cyclic sequences of conformational transitions, so-called motor cycles, that enable them to transform the chemical energy of single ATP molecules into discrete steps along the filament. Two-headed motors walk in a "hand-over-hand" fashion, i.e., by alternating steps in which one head moves forward while the other one remains bound to the filament.

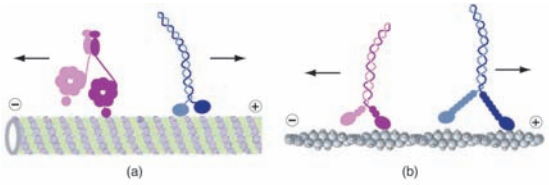

Fig. 1: Molecular motors that bind to and walk along cytoskeletal filaments, which are polar and have two different ends, a "plus" and a "minus" end: (a) Kinesin and dynein that move to the plus and minus end, respectively, of a microtubule; and (b) Myosin V and myosin VI that move to the plus (barbed) and minus (pointed) end, respectively, of an actin filament. The diameter of the microtubule and the actin filament are 25 nm and 8 nm, respectively. For simplicity, the cargo binding domains of the motors have been omitted. All four types of molecular motors are dimers consisting of two identical protein chains and use ATP hydrolysis in order to move in a directed manner. Kinesin and the two myosin motors walk in a "hand-over-hand" fashion.

Each step corresponds to a motor displacement of the order of 10 nanometers, comparable to the size of the motor heads. If there is no shortage of ATP, the motor kinesin, e.g., makes about 100 steps in one second which leads to a velocity of about one micrometer per second. The absolute value of this velocity is not very impressive, but relative to its size, the motor molecule moves very fast: On the macroscopic scale, its movement would correspond to an athlete who runs 200 meters in one second! This is even more surprising if one realizes that the motor moves in a very viscous and noisy environment since it steadily undergoes thermally excited collisions with a large number of water molecules.

Chemical States of Two-Headed Motors

In order to obtain a useful description of such a motor, we can first focus on the different chemical states of the two-headed motor. Each head has a catalytic domain, which is able to hydrolyze ATP into ADP plus P. The corresponding catalytic cycle consists of four subsequent transitions: binding of ATP, hydrolysis of ATP into ADP-P, release of P, and release of ADP. It is convenient to combine ATP hydrolysis and P release into a single transition and to distinguish 3 different states of a single motor head: state (T) with bound ATP, state (D) with bound ADP, or no bound molecule, i.e., empty (E), see **Fig. 2**. The two-headed motor can then attain 3 x 3 = 9 different chemical states and undergo transitions between these states as shown in **Fig.2**. In this figure, each motor state *i* corresponds to the vertex of a network graph. Every pair, *i* and *j*, of states is connected by two directed edges or di-edges corresponding to the forward transition I *ij* > from *i* to *j* and the backward transition I *ji* > from *j* to *i*. In **Fig. 2**, these two di-edges are combined into a single, undirected edge.

In general, the motor may undergo a chemical transition in which one of the catalytic motor domains changes its chemical composition or a mechanical transition corresponding to a mechanical step or substep. For the cytoskeletal motor kinesin, recent experiments indicate that this motor does not exhibit mechanical substeps on the timescale of microseconds **[2]**. In **Fig. 2**, chemical and mechanical transitions are indicated by solid and broken lines, respectively.

The chemical kinetics of the two heads is coordinated: binding of ATP to one head leads to the release of ADP from the other head. The tight coupling of ATP hydrolysis and stepping as well as the hand-over-hand movement indicate that such an out-of-phase behavior of the two heads also governs the catalytic action of stepping kinesin. In order to describe this behavior, we may omit all states in **Fig. 2(a)** for which both heads have the same chemical composition. In this way, we arrive at the reduced state space shown in **Fig. 2(b)** which consists of only six states.

Nonequilibrium Processes and Motor Cycles

Nonequilibrium processes are intimately related to cycles in state space and nonzero fluxes along these cycles. Each cycle, C, consists of two directed cycles or dicycles, C+ and C-, that differ in their orientiation. The network graph in Fig. 2(a) contains a huge number of cycles (more than 200) whereas the one in **Fig. 2(b)** contains only three cycles. Two of these latter cycles, namely <25612> and <52345>, contain both a hydrolysis transition, during which the motor consumes chemical energy, and a mechanical stepping transition, during which the motor can perform mechanical work.

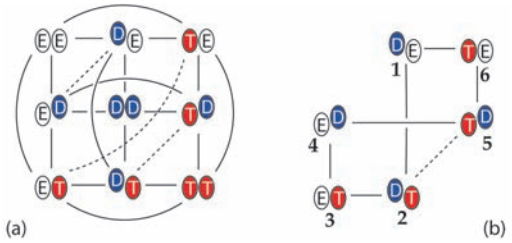

Fig. 2: Network graph with 9 states for a molecular motor with two catalytic domains, each of which can be empty (E), or bind an ATP (T) or ADP (D) molecule. This network contains 21 edges representing 18 chemical forward and backward transitions (solid lines) as well as 3 mechanical forward and backward steps (broken lines); and (b) Reduced state space with 6 states obtained from the 9-state network in (a) by omitting the three states E-E, T-T, and D-D. This network contains 7 edges corresponding to 6 chemical transitions (full lines) plus 1 mechanical transition (broken line).

Steady State Balance Conditions

In our theory, the dynamics of the motor is described by a continuous-time Markov process with transition rates ω_{ij} from state *i* to state *j*. Each dicycle can be characterized, in the steady state of the motor, by a statistical entropy that is produced during the completion of this dicycle **[3]**. Identifying this statistical entropy with the heat released by the motor and using the first law of thermodynamics, we have derived rather general steady state balance conditions of the form

$$k_B T \sum_{ij} \ln(\omega_{ij} / \omega_{ji}) = E_{ch}(C+) - W_{me}(C+)$$

that relate the transition rates ω_{ij} to the chemical energy, $E_{ch}(C+)$, consumed and the mechanical work, $W_{me}(C+)$, performed during the cycle C+. The basic energy scale is provided by the thermal energy $k_B T$, the summation runs over all di-edges $I\ ij >$ of the dicycle C+.

The mechanical work is determined by external load forces experienced by the motor and vanishes in the absence of such forces. This implies that one can decompose the steady state balance conditions into a zero-force and a force-dependent part. In addition, it is straightforward to include other energetic processes into the steady state balance conditions. Two examples are (i) energy input arising from the adsorption of photons and (ii) work against an electrochemical potential. **[3]**

Kinesin's Network of Motor Cycles

In principle, both the transition rates ω_{ij} and the energetic terms on the right hand side of the steady state balance conditions can be measured. If such a complete set of experiments were available for a certain motor, one could use the balance conditions to estimate the experimental accuracy. In practise, some of the transition rates will be difficult to measure, and the balance conditions can then be used to estimate the values of the unknown rates.

We have recently applied this latter strategy to the cytoskeletal motor kinesin **[4]**. One important consequence of our analysis is that the stall force of the motor is determined by the flux balance of two different cycles that govern the forward and backward mechanical step and both involve the hydrolysis of one ATP molecule. This differs from previous unicycle models in which the stall force was determined by the flux balance between the two dicycles of the same cycle. The latter flux balance is, however, not possible for small ADP concentrations as typically considered in motility assays. A detailed comparison between our theory and the experimental data of Ref. **[2]** is shown in **Fig. 3**. In fact, our theory provides a quantitative description for all motor properties as observed in single molecule experiments **[4]**.

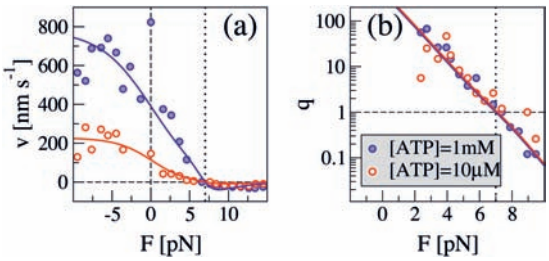

Fig. 3: (a) The motor velocity v and (b) the ratio q of the number of forward to the number of backward mechanical steps as a function of external load force F. The data are for drosophila kinesin and taken from Ref. [2]. The solid lines are calculated using the 6-state network in Fig.2(b). The vertical dotted line corresponds to the stall force at which the velocity vanishes.

R. Lipowsky, S. Liepelt
reinhard.lipowsky@mpikg.mpg.de

References:

[1] Lipowsky, R., Chai, Y., Klumpp, S., Liepelt, S., and Müller, M.J.I., Molecular Motor Traffic: From Biological Nanomachines to Macroscopic Transport, Physica A **372**, 34 (2006).

[2] Carter, N.J. and Cross, R.A.: Mechanics of the kinesin step, Nature **435**, 308 (2005).

[3] Liepelt, S., and Lipowsky, R.: Steady state balance conditions for molecular motor cycles and stochastic nonequilibrium processes, EPL **77**, 50002 (2007).

[4] Liepelt, S., and Lipowsky, R.: Kinesin's network of chemomechanical motor cycles, Phys. Rev. lett. (in press, 2007).

Cooperative Transport by Molecular Motors

Stefan Klumpp 29.09.1973
1999: Diploma, Physics
(University of Heidelberg)
Thesis: Noise-Induced Transport
of Two Coupled Particles
2003: PhD, Physics
(Max Planck Institute of Colloids
and Interfaces, Potsdam)
Thesis: Movements of Molecular
Motors: Diffusion and Directed Walks
Since 2004: Group Leader
(Max Planck Institute of Colloids
and Interfaces, Potsdam)
Since 2006: Postdoc
(University of California, San Diego)

Molecular motors are proteins that transform chemical energy into work and directed movement. Our group is particularly interested in cytoskeletal motors which transport cargoes along the tracks provided by the filaments of the cytoskeleton. Our current understanding of these motors is to a large extent based on biomimetic model systems which consist of only a small number of different components such as motors, filaments, and ATP, the chemical fuel used by these motors. These systems allow us to study molecular motors systematically within a controlled environment.

Important quantities that characterize molecular motors are their velocity and their run length. The latter quantity describes the distance over which the motor moves along the filament before it falls off the track. This run length is typically 1 µm for a single motor molecule. Such unbinding events are unavoidable for molecular motors since they constantly undergo thermal collisions with other molecules.

Cooperative Cargo Transport by Several Motors

In cells, cargo particles such as vesicles and organelles are usually transported by teams of several molecular motors. Because each motor unbinds from and rebinds to the filament, the actual number of motors is not fixed but varies with time. We have developed a model for this type of transport process based on the known properties of single motor molecules **[1]**. This model describes the movement of a cargo particle to which a number N of motors are immobilized. These motors bind to and unbind from a filament in a stochastic manner, so that the number of motors that actually pull the cargo changes stochastically between 1 and N, as shown in **Fig. 1**. The theoretical predictions derived from our model are accessible to in vitro experiments using the same techniques that have been used to study single motors.

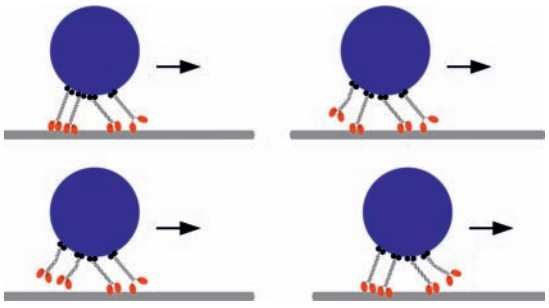

Fig. 1: A cargo particles (blue) is pulled along a filament (grey rod) by four molecular motors. These motors bind to the filament and unbind from it in a stochastic manner, so that the number of actually pulling motors changes between 1 and 4.

The main effect of motor cooperation is an enormous increase in run length, which depends exponentially on the number of motors. We have estimated that 7-8 motors are sufficient for transport over centimetres and that the cooperation of 10 motors leads to run lengths of over a meter **[1]**. Transport over such long distances occurs in the axons of nerve cells, which represents the biggest challenge for long-range transport in cells. The increase in run length has recently been confirmed in experiments done in the group of R. Dimova using latex beads pulled by varying numbers of kinesin motors.

If the cargo is pulled against an opposing force, its movement is slowed down. In addition, the force increases the motors' tendency to unbind from the filament. Since unbinding of motors increases the force that the remaining bound motors have to sustain, this increases their unbinding probability even further and leads to a cascade of unbinding events. As a result of these unbinding cascades, the force-velocity relationship for a cargo pulled by several motors is markedly non-linear, in contrast to the approximately linear force-velocity relations observed for single motors (see **Fig. 2**).

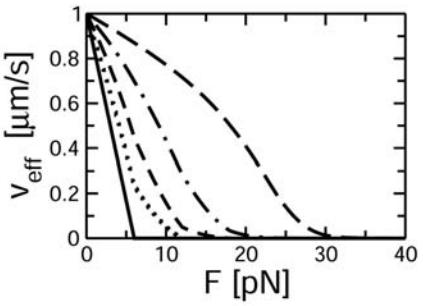

Fig. 2: The force-velocity relation for cargoes transported cooperatively by N motors against an opposing force F. The graph shows curves for N=1,2,3,5, and 10 (from left to right). While the velocity exhibits a linear decrease for a single motor, the curves are non-linear for transport by more than one motor due to the forced decrease of the number of bound motors.

Unbinding cascades also play an important role in systems where cargoes are pulled by two types of motors which move into opposite directions. In that case, the unbinding cascades lead to a tug-of-war-like instability. As a consequence of that instability, the cargo is not stalled by being pulled into opposite directions, but rather switches stochastically between quick runs back and forth **[2]**.

Active Diffusion

Passive diffusion or Brownian motion is too slow to transport larger objects such as vesicles and organelles within cells. This fact is usually taken as an argument for the necessity of active transport. Active transport, however, is not necessarily directed, but can also be used to generate effectively diffusive movements, e.g. if the direction of motion of a motor-driven cargo particles changes from time to time in a random fashion. We call the resulting diffusive, but energy-consuming movements *active diffusion*. There are examples for active diffusion within cells, but active diffusion can also be used in artificial systems as a method to speed up diffusive processes such as the search for an immobile binding partner. Such artificial systems can be expected to have many applications in bionanotechnology. We have studied active diffusion for several systems with regular arrangements of filaments on structured surfaces (see **Fig. 3**) which can be prepared using a number of techniques established during recent years. Our theoretical results indicate that active diffusion is most useful for the transport of large objects – for micron-sized particles in water active diffusion can be 100 times faster than passive Brownian motion – and/or for transport in very viscous environments. Again the cooperation of several motors is helpful, since the maximal active diffusion coefficient that can be generated is proportional to the product of run length and motor velocity.

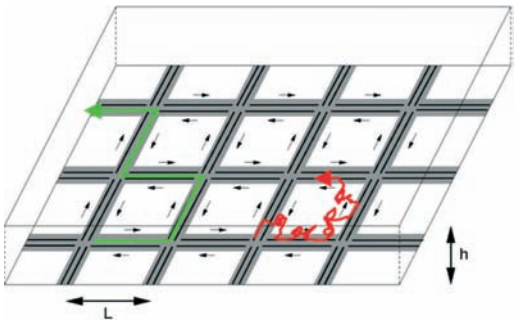

Fig. 3: An array of filaments (black lines) specifically adsorbed on a structured surface. The molecular motor-driven movements along such filament systems exhibit active diffusion, energy-consuming, but effectively diffusive movements as indicated by the green and red trajectories. The characteristic diffusion coefficient of these movements can be much larger than the usual diffusion coefficient which arises from Brownian motion.

Traffic Phenomena

If many molecular motors (or cargo particles pulled by molecular motors) move along the same filament, the traffic may become congested. In contrast to the familiar vehicular traffic jams, however, molecular motors can escape from a congested filament by unbinding from it. We have studied traffic jams of molecular motors that arise from different types of bottlenecks and in different types of compartments **[4]**. In particular, we have recently studied the effect of defects on the filaments and the influence of the compartment geometry on the length of traffic jams. In the latter project, we found that in several types of tube-like compartments, traffic jams are strongly enhanced by the compartment geometry.

S. Klumpp, Y. Chai, M. Müller, R. Lipowsky
klumpp@mpikg.mpg.de

References:

[1] Klumpp, S. and Lipowsky, R.: Cooperative cargo transport by several molecular motors. Proc. Natl. Acad. Sci. USA **102**, 17284-17289 (2005).
[2] Müller, M. J. I., Klumpp, S. and Lipowsky, R.: (to be published)
[3] Klumpp, S. and Lipowsky, R.: Active diffusion by motor particles. Phys. Rev. Lett. **95**, 268102 (2005).
[4] Klumpp, S., Müller, M. J. I. and Lipowsky, R.: Traffic of molecular motors. In: Traffic and Granular Flow '05, edited by Schadschneider, A. et al. (Springer, Berlin 2007), pp.251-261.

Polymerization of Filaments

Julian Charles Shillcock 18.10.1960
1982: B.Sc (Hons), Physics (Kings College London)
1985: M.Sc, Nuclear Physics (Simon Fraser University, Canada)
Thesis: Hanbury-Brown Twiss Effect in Heavy-Ion Collisions
1986-1990: Research Scientist (British Aerospace, Space Systems Division, U.K.)
1995: PhD, Biophysics (Simon Fraser University, Canada)
Thesis: Elastic Properties of Fluid and Polymerised Membranes under Stress
1995-1997: Postdoc (Max Planck Institute of Colloids and Interfaces, Potsdam)
1998-1999: Senior Scientist (Molecular Simulations Inc., Cambridge, U.K.)
1999-2003: Group Leader (Max Planck Institute of Colloids and Interfaces, Potsdam)
2004-2007: External Research Associate (Max Planck Institute of Colloids and Interfaces, Potsdam)

The cytoskeleton of a cell is a major structural component that gives rigidity and support to the plasma membrane and participates in numerous cellular processes. It is composed of rodlike filaments of varying degrees of rigidity that self-assemble, and disassemble, in response to cellular signals. Actin filaments form one part of the cytoskeleton, and are composed of many hundreds of actin monomers that bind together into linear and branched filaments. Each monomer is a globular protein approximately 5 nm in diameter that contains a bound ATP molecule whose hydrolysis, and subsequent phosphorylation, provides the energy required to drive filament growth. In motile cells, actin filaments continually form and disassemble in a process that requires the consumption of ATP. This process is referred to as treadmilling, and is the basis for cell crawling. Although experiments have revealed many fascinating aspects of actin treadmilling in generating cellular motion, the molecular details of the process are still unclear. Molecular Dynamics simulations of small sections of filaments have shown the importance of electrostatic interactions in guiding the monomers onto the ends of the filament, and the kinetics of monomer addition and loss at the two ends of a short filament **[1]**. However, these highly-detailed simulations are limited to short lengths of filament because of their computational cost.

In order to visualize F-actin growth and treadmilling in filaments containing hundreds or thousands of monomers, we are using Brownian Dynamics simulations without an explicit solvent. Each actin monomer moves under the influence of forces between monomers, but has a bulk diffusion coefficient that is a parameter of the simulation. The absence of solvent particles allows simulations of filament growth over times approaching several milliseconds. Actin monomers are represented as polar rigid bodies that diffuse freely around the simulation box and, if they encounter the ends of a filament, can bind to it. The terminal monomers can also unbind from a filament at a constant rate (**Fig. 1**).

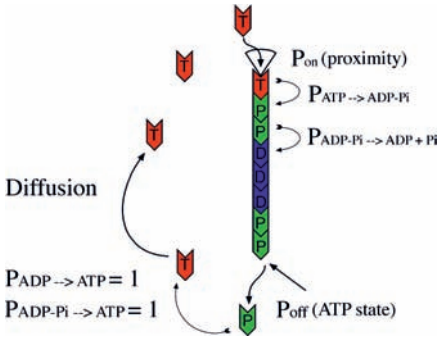

Fig. 1: Diagram showing how the attachment and detachment of actin monomers from a filament is modelled in the simulations. Monomers diffusing in the bulk possess a bound ATP molecule (red monomers). Once a monomer binds to a filament, its ATP molecule has a certain probability of being hydrolysed to ADP with a bound Pi (green monomers). Later, the bound Pi can dissociate leaving the monomer with a bound ADP. The probability for the two terminal monomers of a filament to detach may depend on the monomer's internal state. The ATP molecules are not explicitly modelled in the simulations, but each actin monomer has an internal flag that represents its ATP state. Monomers may be restricted to a single state by setting the probability of ATP hydrolysis to zero, or may be given two states if the probability of the transition from ADP with bound Pi to ADP is set to zero. In the most general case, the internal flag has three states with three transition probabilities. All monomers that detach from a filament are instantaneously converted to ATP monomers as the phosphorylation of the freely-diffusing actin monomers is expected to occur more rapidly than the attachment of monomers to a growing filament in the experiments of interest.

The two ends of F-actin filaments are referred to as the barbed and pointed ends, and are not equivalent. The rates of monomer attachment and detachment are typically different for the two ends, attachment being faster at the barbed end while detachment occurs faster at the pointed end. Monomers have an internal flag that represents the state of a bound ATP molecule: it takes the values ATP, ADP with bound inorganic phosphate, ADP-Pi, and ADP with the phosphate released. The unbinding rates at the filament's ends depend on the terminal monomer's internal state.

Kunkun Guo, a post-doctoral fellow, has been exploring various quantitative measures of a filament's properties and growth behaviour. The stiffness of a single filament is measured from its shape fluctuations in an external potential, and the attachment and loss of actin monomers to a filament is studied as a simple model of treadmilling. Our preliminary results on filament growth are in agreement with previous theoretical models **[2]** in which multiple states of bound ATP/ADP in the actin monomers are required in order to reproduce the observed properties of actin filaments, including the fluctuations in length of a filament as a function of bulk monomer concentration. It currently appears that a filament composed of actin monomers with only one internal ATP state grows tran-

siently but then disintegrates. Monomers that have two internal states appear to show transient periods of treadmilling. A snapshot of a growing filament that consists of monomers with three internal states is shown in **Fig. 2**.

Fig. 2: Snapshot of a growing filament composed of monomers with 3 internal states. The bulk of interior of the filament is made up of monomers with bound ADP (shown in blue) whereas the two ends are composed of monomers with bound ATP (red) or ADP-Pi (green). The sizes of the caps are different at the two ends because the probability of the terminal monomer detaching depends on the state of the monmer, and the precise values are chosen to be different for the two ends.

The bulk of the filament consists of ADP monomers (shown in blue), while the two ends consist of short caps of ADP-Pi (green monomers) and ATP monomers (red). The lengths of the caps, and their proportions of red to green monomers, are different because the detachment probabilities of the monomers depend on the monomer internal state and are chosen to be different at each end to reflect the polar character of actin monomers in the experiments. We are exploring the model's parameter space to see if treadmilling can be observed as a steady-state phenomenon, and to measure quantitative properties of the process **[3]**. **Fig. 3** shows preliminary results for the fluctuating length of a filament composed of monomers with only a single internal state.

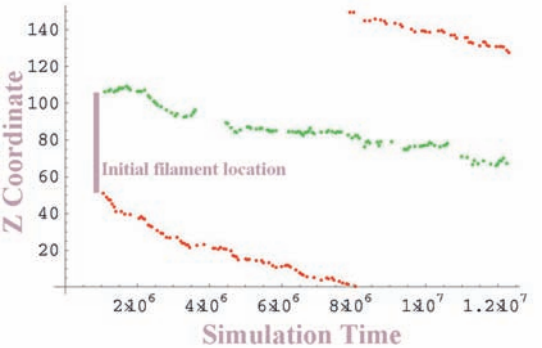

Fig. 3: Plot of the z coordinates of the newly-attached terminal monomers of a growing filament as a function of time. When a monomer attaches to the filament its instantaneous z coordinate is recorded. The two ends of the filament are shown in different colours with the pointed end in green and the barbed end in red, but these do not correspond to the orientation of the barbed and pointed ends shown in Fig. 1. We allow the filament to grow to a certain length before we start measuring its properties. An increasing gap between the two curves indicates that the filament is increasing in length, whereas a decreasing gap shows that it is shrinking. The discontinuity in the red curve at approximately 8,000,000 timesteps is due to the filament extending across the periodic boundary at the z ends of the simulation box.

The filament appears to increase in length continuously throughout the simulation period (the red and green curves move apart). This indicates that this particular filament is not treadmilling. **Fig. 4** shows the distribution of the time intervals between monomer-binding events for the two ends of the same filament as **Fig. 3**. The distribution is approximately exponential, although the relatively small number of data points (65) does not allow a definitive conclusion. This work is continuing.

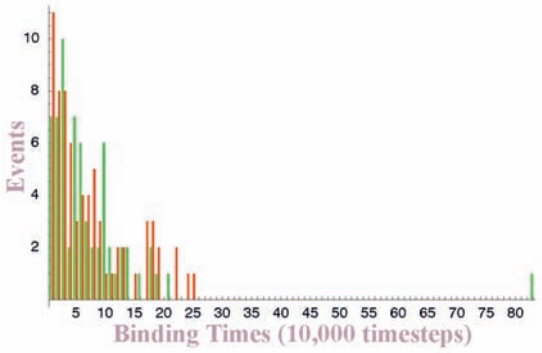

Fig. 4: Histogram of the distribution of time intervals between successive monomers attaching to the two ends of a growing filament (green curve is the filament's pointed end, the red curve is its barbed end). The width of the bins is 10,000 timesteps, and the probability of attachment is seen to be approximately exponentially distributed.

J. C. Shillcock, K. Guo, R. Lipowsky.
Julian.Shillcock@mpikg.mpg.de

References:

[1] Sept, D. and McCammon, J. A., Thermodynamics and kinetics of actin filament nucleation. Biophys. J. **81**, 667-674 (2001).
[2] Vavylonis, D., Yang, Q. and O'Shaughnessy, B. Actin polymerization kinetics, cap structure and fluctuations. PNAS. **102**, 8543-548 (2005).
[3] Guo, K., Shillcock, J. C. and Lipowsky, R. Self-assembly, growth and treadmilling of actin filaments in coarse-grained simulations. JACS. (to be published 2007).

Semiflexible Polymers and Filaments

Jan Kierfeld 31.01.1969
1993: Diploma, Physics
(University of Cologne)
Thesis: On the Existence of the Vortex Glass Phase in Layered Systems
1995-1996: Research Associate
(UC San Diego, California)
1996: PhD, Physics
(University of Cologne)
Thesis: Topological Order and Glassy Properties of Flux Line Lattices in Disordered Superconductors
1997-2000: Postdoc
(Argonne National Laboratory, Illinois)
Since 2000: Group Leader
(Max Planck Institute of Colloids and Interfaces, Potsdam)
2006: Habilitation
(University of Potsdam)
Thesis: Strings and Filaments: From Vortices to Biopolymers

Many biopolymers such as DNA, filamentous (F-) actin or microtubules belong to the class of semiflexible polymers. The biological function of these polymers requires considerable mechanical rigidity. For example, actin filaments are the main structural elements of the cytoskeleton in which actin filaments form a network rigid enough to maintain the shape of the cell and to transmit forces, yet flexible enough to allow for cell motion and internal reorganization in response to external stimuli. Synthetic semiflexible polymers also play an important role in chemical physics. Prominent examples are polyelectrolytes or dendronized polymers, where the electrostatic repulsion of charges along the backbone or the steric interaction of side groups gives rise to considerable bending rigidity.

The bending rigidity of semiflexible polymers is characterized by their persistence length **[1]**, which is given essentially by the ratio of bending rigidity κ and thermal energy. The physics of semiflexible polymers becomes qualitatively different from the physics of flexible synthetic polymers on length scales smaller than the persistence length where bending energy dominates over conformational entropy. Typical biopolymer persistence lengths range from 50nm for DNA to the 10m-range for F-actin or even up to the mm-range for microtubules and are thus comparable to typical contour lengths such that semiflexible behaviour plays an important role.

We theoretically investigate the physics of semiflexible polymers and filaments from the single polymer level to biological structures consisting of assemblies of interacting filaments. This requires exploring the interplay of thermal fluctuations, external forces, interactions, and active fluctuations in filament systems.

Single Filaments:
Fluctuations, Confinement, and Manipulation

The persistence length of a semiflexible polymer gives a typical length scale for its thermal shape fluctuations. The bending energy couples shape fluctuations of different wavelengths. Using a functional renormalization group approach, we calculated how this results in a softening of the polymer with an exponential decay of its bending rigidity for large wavelength fluctuations. This effect provides a concise definition of the persistence length as the characteristic decay length of the bending rigidity **[1]**.

Thermal fluctuations of confined filaments are not only characterized by their persistence length but also by the so-called deflection length, which is related to the confining geometry. In a recent study **[2]** we performed a quantitative fluctuation analysis for actin filaments confined to microchannels and determined both persistence and deflection length.

During the last decade, micromanipulation techniques such as optical tweezers and atomic force microscopy (AFM) have become available which allow the controlled manipulation of single polymers and filaments. Experiments such as pulling single polymers or pushing adsorbed polymers over a surface with an AFM tip open up the possibility of characterizing mechanical filament properties on the single molecule level. In order to interpret such experiments quantitatively, theoretical models are necessary, which we developed for (i) force-induced desorption or unzipping of filaments **[3]** and (ii) the activated dynamics of semiflexible polymers on structured substrates **[4,5]**.

AFM tips or optical tweezers can be used to lift an adsorbed semiflexible polymer from a surface or unzip two bound semiflexible polymers (**Fig.1**). We can calculate the resulting force-extension characteristics for such a force-induced desorption process **[3]**. One interesting feature is the occurrence of an energetic barrier against force-induced desorption or unzipping which is solely due to the effects from bending rigidity (**Fig.1**).

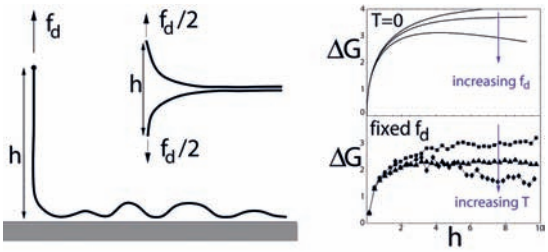

Fig. 1: Left: Force-induced desorption of an adsorbed filament and unzipping of two bound filaments. Right: Free energy landscapes for force-induced desorption as a function of the height h of the polymer end. The polymer desorbs either upon increasing the desorbing force f_d or the temperature T. Both processes are governed by a free energy barrier.

Strongly adsorbed polymers are often subject to surface potentials that reflect the symmetry of the underlying substrate and tend to align in certain preferred directions. If such polymers are pushed over the substrate by point forces as can be exerted by AFM tips, their dynamics is thermally activated and governed by the crossing of the surface potential barriers. Barrier crossing proceeds by nucleation and subsequent motion of kink-antikink pairs (**Fig.2**). The analysis of this process shows that static and dynamic kink properties are governed by the bending rigidity of the polymer and the potential barrier height **[4,5]**.

Structured adsorbed surfaces can also give rise to confinement effects that result in morphological shape transitions of single semiflexible polymers. Currently, we are investigating the morphological diagram for semiflexible polymer rings on a structured substrate containing an adhesive stripe (**Fig.2**). Upon increasing the adhesive potential of the stripe the polymer undergoes a morphological transition from an elongated to a round conformation.

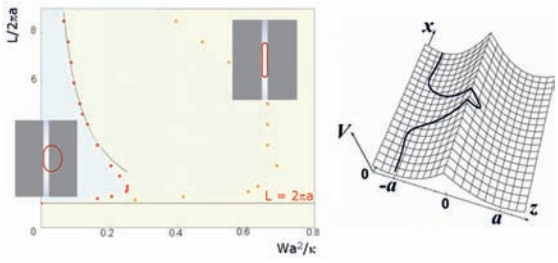

Fig. 2: Right: Kinked conformation of a semiflexible polymer, which is pushed at its mid-point over a potential barrier. Left: Morphological diagram of a semiflexible polymer ring adsorbed on a substrate containing an adhesive stripe of width a as a function of the polymer length L and the ratio of adhesive strength of the stripe and the polymer bending rigidity. In the red region at high adhesive strength, the ring assumes an elongated conformation within the stripe; in the blue region it exhibits a round conformation dominated by bending energy.

Filament Assemblies

Filament assemblies play an important role as functional and structural elements of the cytoskeleton. Using analytical and numerical methods we studied the formation of filament bundles. In the cell, filament bundles are held together by adhesive crosslinking proteins. In a solution of crosslinkers and filaments, the crosslinkers induce an effective attraction between filaments. Starting from analytical results for two filaments, we have studied this problem analytically for N filaments and numerically for up to 20 filaments using Monte-Carlo simulations **[6]**. Above a threshold concentration of crosslinkers a bundle forms in a discontinuous bundling phase transition **[6]**. This mechanism can be used by the cell to regulate bundle formation. Deep in the bundled phase at high crosslinker concentration, we observe a segregation of bundles into smaller sub-bundles, which are kinetically arrested (**Fig.3**). The system appears to be trapped in a glass-like state. Starting from a compact initial state, on the other hand, the bundle reaches its equilibrium configuration with a hexagonal arrangement of filaments (**Fig. 3**).

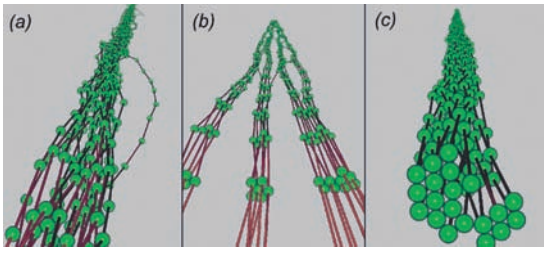

Fig. 3: Three snapshots of a bundle formed by twenty filaments as observed in computer simulations: (a) Loose bundle for a crosslinker concentration that is only slightly above the threshold value; (b) and (c) show two different conformations of the same bundle corresponding to a segregated conformation with three sub-bundles and a compact conformation with roughly cylindrical shape, respectively.

Active Filament Systems

The living cell is an active system where cytoskeletal filaments are not in equilibrium. ATP- or GTP-hydrolysis allows them to constantly polymerise and de-polymerise (treadmilling). For filament bundles, this active polymerisation dynamics can be used for force generation. We found that filament bundles can generate polymerization forces but also zipping forces by converting the gain in adhesive energy upon bundling into a force exerted on a confining wall **[7]**.

Cytoskeletal filaments also interact with molecular motors, which are motor proteins walking on filaments by converting chemical energy from ATP-hydrolysis into mechanical energy. The interplay between filaments and molecular motors can give rise to structure formation far from equilibrium. This can be studied in model systems such as motility assays where motor proteins are immobilized onto a glass plate and actively pull filaments over this surface. Computer simulations and theoretical arguments show that the active driving by molecular motors enhances the tendency of filaments to align: As one increases the density of molecular motors, the system undergoes a phase transition into a nematic liquid crystal (**Fig.4**) **[8,9]**. This ordering effect arises from the interplay of the active driving by molecular motors and steric interactions between filaments. We were able to describe the resulting phase diagram of this non-equilibrium filament system quantitatively in terms of experimentally accessible model parameters by introducing the concept of an effective increased filament length **[8]**. The density of inactive motors and microscopic motor parameters such as detachment and stall forces determine the formation of a new non-equilibrium phase, a kinetically arrested cluster phase with mutually blocking filaments **[9]**.

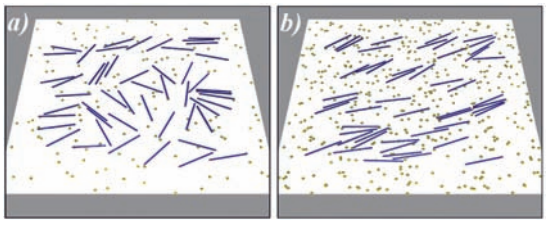

Fig. 4: Two snapshots of rodlike filaments (blue) on a surface coated with immobilized molecular motors (yellow). (a) At low motor surface density the filaments display no order. (b) Above a threshold value for the motor density, the filaments spontaneously order into a parallel pattern. This "active nematic ordering" is caused by the interplay of filament collisions and their motor-driven motion.

J. Kierfeld, K. Baczynski, K. Goldammer, P. Gutjahr, T. Kühne, P. Kraikivski
Jan.Kierfeld@mpikg.mpg.de

References:

[1] Gutjahr, P., Lipowsky, R., Kierfeld J.: Persistence length of semiflexible polymers and bending rigidity renormalization. Europhys. Lett. **76**, 994-1000 (2006).

[2] Köster, S., Stark, H., Pfohl, T., Kierfeld, J.: Fluctuations of Single Confined Actin Filaments, Biophys. Rev. Lett., in press (2007).

[3] Kierfeld, J.: Force-Induced Desorption and Unzipping of Semiflexible Polymers, Phys. Rev. Lett. **97**, 058302 (2006).

[4] Kraikivski, P., Lipowsky, R., Kierfeld, J.: Activated dynamics of semiflexible polymers on structured substrates, Eur. Phys. J. E **16**, 319-340 (2005).

[5] Kraikivski, P., Lipowsky, R., Kierfeld, J.: Point force manipulation and activated dynamics of semiflexible polymers on structured substrates, Europhys. Lett. **71**, 138-144 (2005).

[6] Kierfeld, J., Kühne, T., Lipowsky, R.: Discontinuous unbinding Transitions of Filament Bundles, Phys. Rev. Lett. **95**, 038102 (2005).

[7] Kierfeld, J., Gutjahr, P., Kühne, T., Kraikivski, P., Lipowsky, R.: Buckling, Bundling, and Pattern Formation: From Semi-Flexible Polymers to Assemblies of Interacting Filaments, J. Comput. Theor. Nanosci. 3, 898-911 (2006).

[8] Kraikivski, P., Lipowsky, R., Kierfeld, J.: Enhanced Ordering of Interacting Filaments by Molecular Motors, Phys. Rev. Lett. **96**, 258103 (2006).

[9] Kierfeld, J., Kraikivski, P., Lipowsky, R.: Filament Ordering and Clustering by Molecular Motors in Motility Assays, Biophys. Rev. Lett. 1, 363-374 (2006).

Fractionation and Low-Density-Structures in Systems of Colloidal Rods

Thomas Gruhn 10.06.1969
1995: Diploma, Physics (Technische Universität Berlin)
Thesis: Monte-Carlo-Untersuchungen der Ausrichtung nematischer Flüssigkristalle (A Monte Carlo study of the alignment in nematic liquid crystals)
1998: PhD, Physics (Institut für Theoretische Physik, TU Berlin)
Thesis: Substrate-induced order in confined molecularly thin liquid-crystalline films
1999: R&D Project (Siemens AG, Berlin)
2000: Postdoc (University of Massachusetts, USA)
2001: Group Leader (Max Planck Institute for Colloids and Interfaces, Potsdam)

Rigid rods of mesoscopic size can nowadays be synthesized in large amounts. Examples are carbon nanotubes, boehmite needles, cylindrical dendrimers, and metallo-supramolecular polyelectrolytes (see references in **[1]**). Colloidal rods are of great relevance for the creation of mesoscopic structures. In solution they can self-organize and induce long-range spatial and orientational order. Typical examples are liquid-crystalline mesophases, known from systems of small liquid crystal molecules. There are, however, important differences between traditional liquid crystals and systems of mesoscopic rods. While systems of small liquid crystal molecules are typically monodisperse or consist of a small number of components, most systems of synthesized colloidal rods have a polydisperse length distribution, due to the production method. Furthermore, the alignment of small rods is mainly caused by a coupling of the molecules' polarization axes, while orientational order of mesoscopic rods is typically based on steric interactions. Therefore, in many cases colloidal rods can be successfully approximated as hard spherocylinders. However, if van-der-Waals forces between the colloidal rods cannot be neglected or if the solvent generates strong depletion forces between adjacent rods, attractive interactions must be considered.

Fractionation in Systems of Chemically Homogenous Rods

Polydisperse systems of spherocylindrical rods have a pressure range in which an isotropic phase with no orientational order coexists with a phase which is (at least) orientationally ordered. In this case, long rods are preferentially found in the ordered phase while the majority of small rods is located in the isotropic phase. With the help of Monte Carlo simulations we have investigated the influence of attractive interactions on fractionation effects in a polydisperse system of spherocylinders **[2]**. A spherocylinder consists of a cylinder of diameter D and length $L=\lambda D$, which is capped by two hemispheres with diameter D. We analyzed a polydisperse system of rods with cylinder lengths between $\lambda=1$ and $\lambda=8$ for various reduced pressures $P^*=Pv_{av}/T$, where v_{av} is the average rod volume and T is the thermal energy including the Boltzmann factor k_B. At large pressures long rods are strongly aligned while the orientational order for short rods is low. The discrepancy between the order of short and long rods is strongly enhanced by attractive interactions (**Fig. 1**).

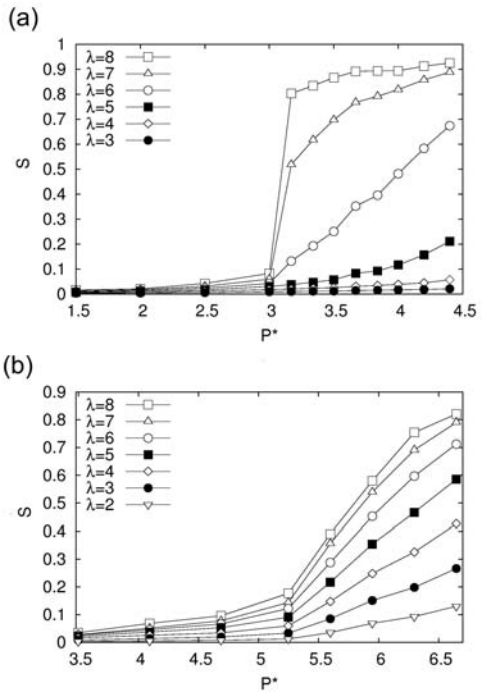

Fig. 1: Orientational order parameter S of components with cylinder length λ in a polydisperse rod system at reduced pressure P. (a) In a system of attractive rods, long rods are strongly aligned at pressures P*>3, while short rods are almost isotropic.(b) For hard rods), the orientational order decreases gradually with the rod length.*

An analysis of the local structure reveals that, at high pressures, long attractive rods form a smectic monolayer with hexatic in-plane order, while hard rods form a less ordered nematic droplet which consists of preferentially long rods (cmp. **Fig. 2**).
This corresponds to experimental results for fd-viruses in a polymer solution which form strongly ordered mono-layers in the presence of strong depletion forces and less ordered domains if depletion forces are weak **[3]**.

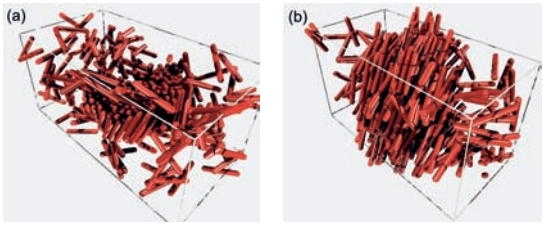

Fig. 2: Typical configurations for polydisperse systems of (a) attractive and (b) hard rods. For clarity reasons short rods (λ<5) are omitted. In (a) long rods aggregate to a smectic monolayer, in (b) a nematic droplet forms.

Spatial fractionation can also be induced by an adjacent, structured substrate. For this purpose, substrates with rectangular cavities turned out to be particularly suited. **Fig. 3** shows configurations of an equilibrated rod system with four different lengths in contact with a substrate with cavities of different sizes. Starting from a random configuration, the different rods aggregate inside the corresponding cavities. Long rods form a smectic monolayer which grows out of the substrate cavities.

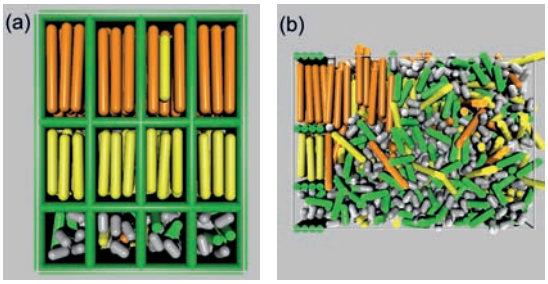

Fig. 3: Typical configurations for a system of rods with four different lengths in contact with a structured substrate with rectangular cavities of different sizes. Molecules demix and aggregate in the corresponding cavities as shown in (a) from the planar substrate (not shown) behind the cavities and (b) in a side view.

Low-Density Structures in Systems of Chemically Heterogenous Rods

Additional types of structures can form in systems of chemically heterogenous rods. We have studied rods with one or two short-range adhesive sites along the molecule axis which can adhere to sites of other rods **[4]**. Typical examples are stiff block-copolymers where the hydrophobic parts aggregate to screen themselves from the surrounding water. The chemically heterogenous rods form complex structures at rather low densities. Hard rods with one adhesive segment located halfway between the center and the end of the rod may form membrane-like clusters (**Fig. 4a**). For entropic reasons half of the rods point up and half point downward, resulting in a membrane of width $w \approx 3L/2$. If the adhesive segment is located at the end of the rods, micellar structures are formed (**Fig. 4b**).

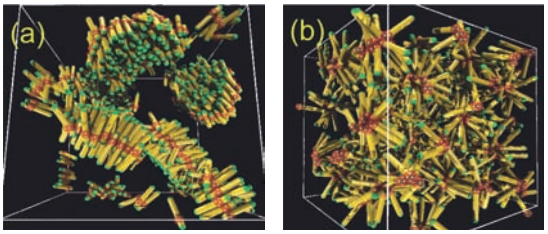

Fig. 4: Snapshots of hard rods with one adhesive segment (a) half way between the center and the end of the rod and (b) at the end of the rod.

The system behaves completely different if adhesive sites are located on both ends. For this type of rods with length $\lambda = 5$, we have estimated a phase diagram as a function of the reduced pressure P^* and the adhesive strength ε (**Fig. 5**). For small ε, the system shows an isotropic and a nematic state, just like a system of hard rods. For sufficiently large ε and low pressure a novel scaffold-like state is found with a flexible network of rods. The scaffold state is characterized by triangular structures formed by three mutually adhering rods. At higher pressures, small smectic-like bundles occur, before at even higher pressure a long-range smectic order sets in.

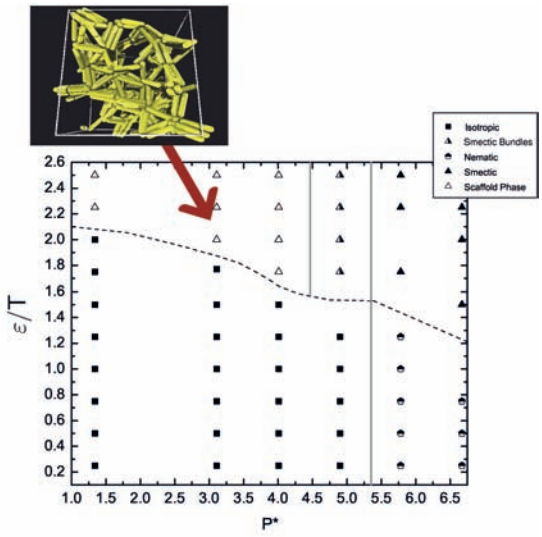

Fig. 5: Phase diagram of a system of hard rods with adhesive ends. For sufficiently high adhesion strength ε and low reduced pressure P the system forms a scaffold-like structure as shown in the snapshot on top.*

T. Gruhn, R. Chelakkot, E. Gutlederer, A. Richter.
thomas.gruhn@mpikg.mpg.de

References:

[1] Richter, A. and Gruhn, T.: Fractionation in polydisperse systems of spherocylindrical rods – The influence of attractive interactions and adjacent substrates, Mol. Phys. **104**, 3693-3699 (2006).
[2] Richter, A. and Gruhn, T.: Structure formation and fractionation in systems of polydisperse rods, J. Chem. Phys. **125**, 064908 (2006).
[3] Dogic, Z. and Fraden, S.: Development of model colloidal liquid crystals and the kinetics of the isotropic-smectic transition, Phil. Trans. R. Soc. Lond. A **359**, 997-1014 (2001).
[4] Chelakkot, R., Lipowsky, R., and Gruhn, T.: Novel low-density structure for hard rods with adhesive end-groups, Macromolecules **39**, 7138-7143 (2006).

Exploring Vesicle Fusion with Dissipative Particle Dynamics

Julian Charles Shillcock 18.10.1960
1982: B.Sc (Hons), Physics (Kings College London)
1985: M.Sc, Nuclear Physics (Simon Fraser University, Canada) Thesis: Hanbury-Brown Twiss Effect in Heavy-Ion Collisions
1986-1990: Research Scientist (British Aerospace, Space Systems Division, U.K.)
1995: PhD, Biophysics (Simon Fraser University, Canada) Thesis: Elastic Properties of Fluid and Polymerised Membranes under Stress
1995-1997: Postdoc (Max Planck Institute of Colloids and Interfaces, Potsdam)
1998-1999: Senior Scientist (Molecular Simulations Inc., Cambridge, U.K.)
1999-2003: Group Leader (Max Planck Institute of Colloids and Interfaces, Potsdam)
2004-2007: External Research Associate (Max Planck Institute of Colloids and Interfaces, Potsdam)

Computer models of biophysical processes are important both for understanding their generic features and for visualizing their dynamics **[1]**. Many interesting phenomena occur on length and time scales beyond the reach of traditional Molecular Dynamics (MD), and this has led to the development of so-called *mesoscopic* simulation methods. We have been using Dissipative Particle Dynamics (DPD) to construct improved models of amphiphilic membranes and explore the pathway of vesicle fusion. We have recently published an invited review of simulation methods applied to these soft matter systems **[2]**. Natural membranes, such as the cellular plasma membrane, are a complex mixture of many types of lipid molecule and protein. We have continued to study the material properties of amphiphilic membranes as models of lipid bilayers. The effects of molecular architecture **[3]** and a mixture of two molecule types with different tail lengths and intermolecular interactions **[4]** have been simulated using DPD (**Fig. 1**) by Gregoria Illya (now a post-doc at the MPI for Polymer Research in Mainz). The elastic properties of a membrane composed of two lipid species was also simulated **[5]** using coarse-grained Molecular Dynamics by Alberto Imparato (now a post-doc at the Politecnico di Torino in Torino, Italy). The two techniques produced similar results, indicating that the membrane properties are robust against changing the details of the simulation techniques.

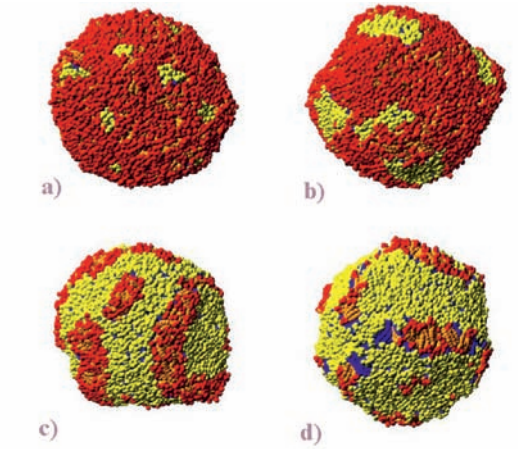

Fig. 1: Phase separation in a vesicle composed of two kinds of lipid with different hydrophobic tail lengths as a function of the longer-tailed lipid concentration (from [4]). The shape of the domains differs from those formed in planar bilayers containing the same lipid types and concentrations because the curvature of the vesicle influences the domain growth. The number fractions of the longer-tail lipid (shown with yellow heads) are as follows: a) 0.1, b) 0.3, c) 0.7, and d) 0.9. The shorter-tail lipids are shown with red heads.

A quite different class of vesicle-forming amphiphiles consists of diblock copolymers, such as poly(ethylene oxide)-polyethylethylene (PEO-PEE). These materials are important for applications such as drug delivery because they form vesicles that are more robust than lipid vesicles, and are not recognised as foreign by the human immune system. In collaboration with the groups of Professors M. Klein and D. Discher at the University of Pennsylvania, we have created a DPD model of PEO-PEE membranes and vesicles and calibrated the DPD parameters using MD simulations on smaller systems **[6]**. This illustrates one way of extending the more accurate, but far more computationally-expensive, MD technique to molecules and system sizes closer to biologically-relevant processes. One application, performed by the Discher group using our DPD code, is to the behaviour of stable pores in the nuclear membrane **[7]**.

Vesicle fusion is a vital cellular function, but the molecular rearrangements that occur when intact membranes approach, merge and fuse cannot yet be observed in experiments. We have extended our previous model **[8]** of tension-induced fusion in two independent ways. The first method replaces the global tensions in the membranes with local forces exerted by transmembrane barrel "proteins" that transduce forces into the membranes (**Fig. 2**).

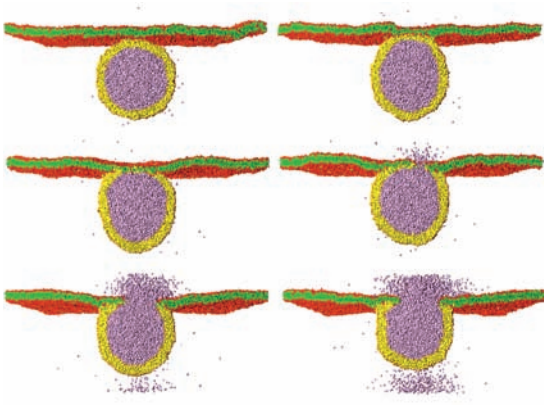

Fig. 2: Sequence of snapshots showing the fusion of a 28 nm diameter vesicle (yellow/orange beads) to a (100 nm)^2 planar membrane (green/red beads). Time proceeds across each row (from [2]). Both membranes are tensionless, and their fusion is driven by local forces exerted by membrane-spanning barrel "proteins". Six barrels are positioned in each membrane in an hexagonal arrangement. A specific force protocol is applied to the barrels to drive the membranes to fuse. After the system has equilibrated, oppositely-oriented bending moments are created in each membrane for 80 ns to bend them towards each other. When the membranes' proximal leaflets have touched, the bending moments are removed and the system is allowed to evolve for 32 ns in order for the two proximal leaflets to merge somewhat. An external force is then applied to the barrels in both membranes so as to raise the tension in the encircled contact zone. The force has a magnitude Fext = 0.4 k_BT/a_0 and is directed radially outward (a_0 is the bead diameter). It is applied in this instance for 64 ns. Once the pore has appeared, it initially expands under the pressure of the inner solvent flowing outwards, but as the membrane relaxes back to its tensionless state it shrinks.

The second method retains the global tensions as the control parameters, and uses a systematic exploration of new parameter sets to develop a more accurate representation of the membrane's mechanical properties (**Fig. 3**). One such parameter set **[9]** was introduced by Lianghui Gao (a post-doc now in Beijing, China) and shows that finite-size effects must be carefully assessed before the model can be compared with experimental systems. This result is important for the development of simulations of many soft matter systems. Lianghui Gao and Andrea Grafmüller, a PhD student, have independently produced two new membrane parameter sets that reveal more details about the pathway of tension-induced vesicle fusion. Key features of these parameter sets are that the membrane is less stretchable than before, and the relation between its tension and area per molecule is linear over the whole range of tensions for which the membrane is intact.

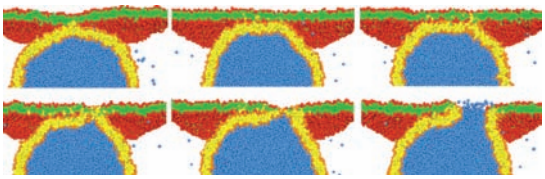

Fig. 3: Fusion pathway of a 30 nm diameter vesicle (yellow/orange beads) to a (50 nm)^2 planar membrane (green/red beads) driven by tension. Time proceeds across each row (from [10]). The stages of fusion are: adhesion of vesicle to membrane (snapshot 2); flip-flop of lipids from the vesicle to the planar membrane (snapshot 3); formation of a disordered, irregularly-shaped contact zone (snapshot 4); transformation of part of the contact zone into a hemifused lamella state (snapshot 5); rupture of the hemifused patch and growth of the fusion pore (snapshot 6).

Andrea Grafmüller has used one of the new parameter sets **[10]** to simulate the fusion of a vesicle to a planar membrane (**Fig. 3**). Both small, 15 nm diameter, and large, 30 nm diameter, vesicles have been followed as they interact with a planar membrane patch that is 50 x 50 nm^2. These simulations have revealed that the fusion of a relaxed vesicle to a tense membrane passes through two energy barriers. The first corresponds to the time required for individual lipid molecules to flip-flop from the (relaxed) vesicle to the (tense) planar membrane; and the second to the appearance of the fusion pore in a bean-shaped disordered region created by the mingling of vesicle and planar membrane lipids. This result may be important for interpreting fusion experiments as most theoretical models to date assume a single energy barrier in the fusion pathway.

J. C. Shillcock, L. Gao, A. Grafmüller, R. Lipowsky.
Julian.Shillcock@mpikg.mpg.de

References:

[1] Shillcock, J. C. and Lipowsky, R. Visualizing soft matter: mesoscopic simulations of membranes, vesicles and nanoparticles. Biophys. Reviews and Letters, Vol 2 No.1, 33-55 (2007).
[2] Shillcock, J. C. and Lipowsky, R. The computational route from bilayer membranes to vesicle fusion. J. Phys. Cond. Mat. **18**, S1191-S1219 (2006).
[3] Illya, G., Lipowsky, R. and Shillcock, J. C. Effect of chain length and asymmetry on material properties of bilayer membranes. J. Chem. Phys. **122**, 244901-1-244901-6 (2005).
[4] Illya, G., Lipowsky, R., and Shillcock, J. C. Two-component membrane material properties and domain formation from dissipative particle dynamics. J. Chem. Phys. **125**, 114710-1-114710-9 (2006).
[5] Imparato, A., Shillcock, J. C. and Lipowsky, R. Shape fluctuations and elastic properties of two-component bilayer membranes. Europhys. Lett. **69**, 650-656 (2005).
[6] Ortiz, V., Nielsen, S. O., Discher, D. E, Klein, M. L., Lipowsky, R., and Shillcock, J. C. Dissipative particle dynamics simulations of polymersomes. J. Phys. Chem. B **109**, 17708-17714 (2005).
[7] Photos, P. J., Bermudez, H., Aranda-Espinoza, H, Shillcock, J. C. and Discher D. E. Nuclear pores and membrane holes: generic models for confined chains and entropic barriers in pore stabilization. Soft Matter **3**, 1-9 (2007).
[8] Shillcock, J. C. and Lipowsky, R. Tension-induced fusion of membranes and vesicles. Nature Materials **4**, 225-228 (2005).
[9] Gao, L., Shillcock, J. C. and Lipowsky, R. Improved dissipative particle dynamics simulations of lipid bilayers. J. Chem. Phys. (accepted 2006).
[10] Grafmüller, A., Shillcock, J. C. and Lipowsky, R. Pathway of membrane fusion with two energy barriers. Phys. Rev. Lett. (accepted 2007).

Unveiling Membrane Fusion

Rumiana Dimova 06.04.1971
1995: Diploma, Chemistry (Sofia University, Bulgaria), Major: Chemical Physics and Theoretical Chemistry, Thesis: Role of the Ionic-Correlation and the Hydration Surface Forces in the Stability of Thin Liquid Films
1997: Second MSc (Sofia University, Bulgaria) Thesis: Interactions between Model Membranes and Micron-Sized Particles
1999: PhD, Physical Chemistry (Bordeaux University, France) Thesis: Hydrodynamical Properties of Model Membranes Studied by Means of Optical Trapping Manipulation of Micron-Sized Particles
2000: Postdoc (Max Planck Institute of Colloids and Interfaces, Potsdam)
Since 2001: Group Leader (Max Planck Institute of Colloids and Interfaces, Potsdam)

Membrane fusion is an essential and ubiquitous cellular process. It is involved, for example, in cellular secretion via exocytosis, signalling between nerve cells, and virus infection. In both the life sciences and bioengineering, controlled membrane fusion has many possible applications, such as drug delivery, gene transfer, chemical microreactors, or synthesis of nanomaterials. While previous studies have explored many of the steps involved in membrane fusion, the efforts to fully understand the dynamics of membrane fusion have been stymied by the speed with which this process occurs.

Recently, our lab has succeeded in the development of two independent methods of initiating the fusion process in a controlled manner. This, in turn enabled us to observe the subsequent fusion dynamics, using phase contrast microscopy and a fast digital camera, with a temporal resolution in the microsecond range **[1]**. This time resolution is unprecedented, as direct observations of fusion in the literature access only times larger than several milliseconds.

The fusion process was observed on giant unilamellar vesicles (~ several tens of micrometers in diameter). In the first protocol **[2]**, the vesicles were functionalized with synthetic fusion-triggering molecules (β-diketonate ligands). Then, two of these liposomes were aspirated into two glass micropipettes. Membrane fusion was subsequently induced by the local addition of ions that form a complex between two fusogenic molecules embedded in the opposing membranes; see **Fig. 1**.

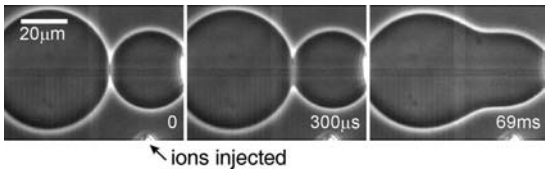

Fig. 1: Snapshots from the fusion of two functionalized vesicles held by micropipettes (only the right pipette tip is visible on the snapshots). A third pipette (bottom right corner) is used to inject a small volume (few tens of nanoliters) of solution of $EuCl_3$ which triggers the fusion. The time after the beginning of the fusion process is indicated in the lower right corner.

In the second protocol, two lipid vesicles were brought into contact by weak alternating electric fields. The AC field served to line up the vesicles along the direction of the field. Thus, while the micropipettes were used to manipulate the vesicles in the first protocol, the AC field was the manipulation tool in the second one. Once close contact was established, membrane fusion was induced by exposing the vesicles to a strong electric pulse. Such a pulse leads to the formation of membrane pores **[3]** in the opposing membranes, which subsequently fuse in order to dispose of the edges of the pores. In the presence of salt in the vesicle exterior, the vesicles deform to acquire cylindrical shapes with round caps **[4]**. In the absence of salt, this curious deformation is not observed, and multiple fusion necks are formed in contrast to the no-salt case where a single fusion neck is formed; see **Fig. 2**.

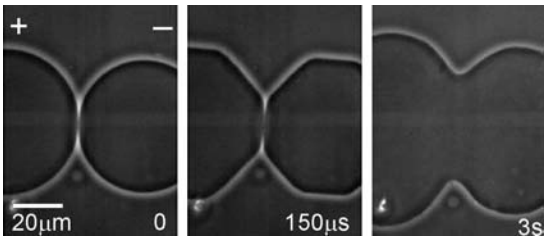

Fig. 2: Snapshot series from the electrofusion of two vesicles. The polarity of the electrodes is indicated with a plus (+) or a minus (-) sign on the first snapshot. The amplitude of the pulse was 150 V (3 kV/cm), and its duration was 150 μs. The starting time t = 0 corresponds to the beginning of the pulse. The image acquisition rate was 20 000 frames per second. The external vesicle solution contained 1 mM NaCl, which causes the flattening of the vesicle membrane and induce cylindrical deformation [4].

With either method, ligand mediated fusion or electrofusion, the process was recorded using a fast digital camera with an acquisition rate of 20 000 frames per second, corresponding to a temporal resolution of 50 microseconds. This constitutes a 1000-fold improvement compared to other direct-observation microscopy reports on fusion. The direct imaging provided by the two fusion protocols and the fast acquisition speed confirmed that the fusion process is extremely fast, and offered some insight into the dynamics of the process. The improved temporal resolution suggests that for the formation of a fusion neck, the cell needs only a few hundred nanoseconds. Within 50 microseconds, the fusion neck connecting the two vesicles was observed to have already reached a diameter of a few micrometers **[1]**. This suggests that the opening of the fusion pore occurs with an expansion velocity of a few centimeters per second. The experimental data could be extrapolated to shorter times covered by simulation studies performed in our department. The latter nicely support the conjecture that fusion times are on the order of 200 nanoseconds.

Having demonstrated the potential of the method for controlling and imaging membrane fusion, we applied it to a slightly more sophisticated system. Namely, we fused two vesicles whose membranes were composed of different lipids (Dioleoylphosphocholine and Sphingomyelin) and cholesterol. At a certain temperature, these lipids form fluid phases, also known as liquid ordered and liquid disordered. These phases are immiscible and the liquid ordered phase, which is stabilized by cholesterol, is thought to mimic rafts in cell membranes.

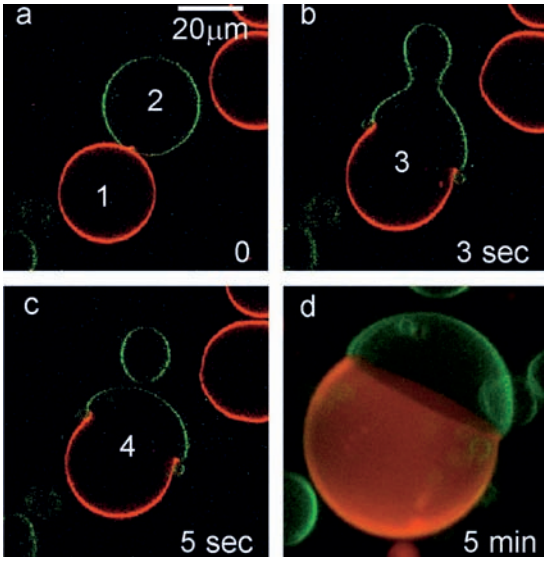

Fig. 3: Creating a multidomain vesicle by electrofusion of two vesicles of different composition as observed with fluorescence microscopy. The images (a-c) are acquired with confocal microscopy scans nearly at the equatorial plane of the fusing vesicles. (a) Vesicle 1 is composed of Dioleoylphosphocholine:Cholesterol (8:2) and labeled with the fluorescent dye DiI-C_{18} (red). Vesicle 2 is made of Sphingomyelin:Cholesterol (7:3) and labeled with the fluorescent dye perylene (green). (b) The two vesicles were subjected to an electric pulse of strength 300 V (6 kV/cm) and duration 300 μs. Vesicles 1 and 2 have fused to form vesicle 3. (c) Right after the fusion, the Sphingomyelin:Cholesterol part (green) begins to bud forming a small daughter vesicle. (d) A three-dimensional image projection of vesicle 4.

When two such vesicles are forced to fuse, the resulting vesicle contains two or more domains. We used the electrofusion protocol to form these multidomain vesicles **[5]**. The fusion products were explored using confocal microscopy, see **Fig. 3**. Having the tool to form these domains on vesicles in a controlled fashion would allow us to study their stability at various conditions like temperature and membrane tension (PhD project of Natalya Bezlyepkina).

In conclusion, we have achieved controlled fusion induced by two approaches: ligand mediated fusion and electrofusion. The tools available in our lab have allowed us to reach unprecedented time resolution of the fusion process. Being able to control fusion, we used our approach to form multidomain vesicles and study the stability of the domains. Currently we apply the electrofusion of giant vesicles as a tool to create microreactors with very small volumes (postdoctoral project of Peng Yang). The vesicles used in the present study were only tens of microns in size. Fusing two of these vesicles of different content would be equivalent to performing a reaction in a tiny volume of some picoliters, which would be advantageous for synthesis of nanomaterials. Furthermore, vesicles as microscopic vessels loaded with polymer solutions can be used to study phase separation in confined systems (PhD project of Yanhong Li), which mimics microcompartmentation in cells.

R. Dimova, N. Bezlyepkina, C. Haluska,
Y. Li, K. A. Riske, P. Yang
Rumiana.Dimova@mpikg.mpg.de

References:

[1] Haluska, C. K., Riske, K. A., Marchi-Artzner, V., Lehn, J.-M., Lipowsky R. and Dimova, R.: Timescales of membrane fusion revealed by direct imaging of vesicle fusion with high temporal resolution. Proc. Natl. Acad. Sci. USA. **103**, 15841-15846 (2006).

[2] Haluska, C. K.: Interactions of functionalized vesicles in the presence of Europium (III) Chloride. PhD Thesis, (2005).

[3] Riske, K. A. and Dimova, R.: Electro-deformation and -poration of giant vesicles viewed with high temporal resolution. Biophys. J., **88**, 1143-1155 (2005).

[4] Riske, K. A. and Dimova, R.: Electric pulses induce cylindrical deformations on giant vesicles in salt solutions. Biophys. J. **91**, 1778-1786 (2006).

[5] Riske, K. A., Bezlyepkina, N., Lipowsky, R. and Dimova, R.: Electrofusion of model lipid membranes viewed with high temporal resolution. Biophys. Rev. Lett. **4**, 387-400 (2006).

Electro-Deformation and -Poration of Vesicles

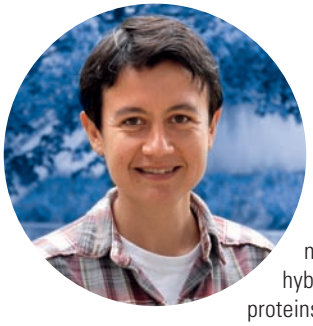

Rumiana Dimova 06.04.1971
1995: Diploma, Chemistry (Sofia University, Bulgaria), Major: Chemical Physics and Theoretical Chemistry, Thesis: Role of the Ionic-Correlation and the Hydration Surface Forces in the Stability of Thin Liquid Films
1997: Second MSc (Sofia University, Bulgaria) Thesis: Interactions between Model Membranes and Micron-Sized Particles
1999: PhD, Physical Chemistry (Bordeaux University, France) Thesis: Hydrodynamical Properties of Model Membranes Studied by Means of Optical Trapping Manipulation of Micron-Sized Particles
2000: Postdoc (Max Planck Institute of Colloids and Interfaces, Potsdam)
Since 2001: Group Leader (Max Planck Institute of Colloids and Interfaces, Potsdam)

The response of membranes to electric fields has been extensively studied in the last decades. The phenomena of electrodeformation, electroporation and electrofusion are of particular interest because of their widespread use in cell biology and biotechnology as means for cell manipulation, cell hybridization or for introducing molecules such as proteins, foreign genes (plasmids), antibodies, or drugs into cells. Giant vesicles are the simplest model of the cell membrane. Being of cell size, they are convenient for direct microscopy observations.

Deformation in AC Fields

When subjected to alternating electric fields, giant vesicles deform into elliptical shapes. The deformation depends on the AC field frequency and on the conductivities of the aqueous solution in the interior and exterior vesicle compartments **[1]**. When the interior solution has conductivity (σ_{in}) higher than the exterior one (σ_{out}), a quasispherical vesicle deforms into a prolate. This deformation is observed for a large range of AC frequencies, up to 10^6 Hz. Interestingly, whenever the internal conductivity is lower than the external one ($\sigma_{in} < \sigma_{out}$), as in **Fig. 1**, a prolate-oblate transition (**Fig. 1a** and **1b**) is observed for intermediate frequencies of a few kHz. This applies also to external conductivities close to physiological conditions. At higher frequencies, more than about 10^7 Hz, the vesicles attain a spherical shape (**Fig. 1c**) irrespective of conductivity conditions; see **Fig. 2**.

Fig. 1: A giant vesicle (phase contrast microscopy) subjected to an AC field of 10 V (2 kV/cm). The field direction is indicated with the arrow in (a). The external solution has a higher conductivity than the internal one ($\sigma_{in} > \sigma_{out}$). From (a) to (c) the field frequency increases causing shape transformations of the vesicle: (a) 5 kHz, prolate morphology; (b) 100 kHz, oblate shape; (c) 10 MHz, sphere.

Using giant unilamellar vesicles made of egg PC, we succeeded to map the morphological transitions as a function of AC frequency and conductivity ratios. The conductivities were varied by the addition of NaCl (leading to concentration of up to about 1 mM) in the exterior or interior vesicle solutions. A large interval of frequencies was studied (up to 10^8 Hz). The degree of vesicle deformation was quantitatively characterized from optical video microscopy images.

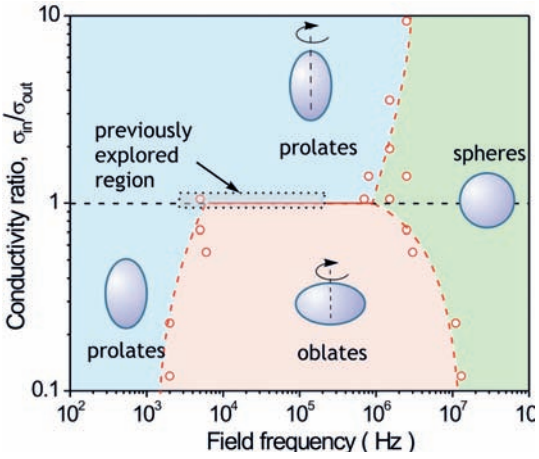

Fig. 2: Morphological diagram of the shape transformations of vesicles in different conductivity conditions and various field frequencies. When the conductivity of the solution inside the vesicles is larger than the one outside, ($\sigma_{in} > \sigma_{out}$), transitions from prolate to spherical vesicles are observed (upper part of the diagram). For internal conductivities lower than the external one ($\sigma_{in} > \sigma_{out}$), the vesicle undergoes prolate-to-oblate-to-sphere transitions depending on the field frequency (lower part of the diagram). The open circles are experimentally determined. The dashed lines are guides to the eye for the various region boundaries. The area surrounded by the dotted line shows the region previously explored in the literature.

Earlier studies by Helfrich and collaborators (see e.g. Winterhalter and Helfrich, *J. Coll. Interf. Sci.* 122, 1987) report on prolate deformations of vesicles in AC fields, but conductivity asymmetry has not been studied and thus not taken into account in the theoretical modelling. Thus the transition observed in our system cannot be predicted by the existing theory. We extended these theories to include the effect of asymmetric conductivity conditions and the frequency dependence of the conductivity (PhD project of Said Aranda).

Electroporation of Vesicles Subjected to DC Pulses

When subjected to short and strong electric pulses (~100 µs, ~1 kV/cm) the vesicle response is qualitatively similar to the one in AC fields. However, microscopy observation of effects caused by electric pulses on giant vesicles is difficult because of the short duration of the pulses. To tackle this problem, recently in our group, imaging with a fast digital camera was used to record the pulse response of giant lipid vesicles with a high temporal resolution of up to 30 000 frames per second (one image every 33 microseconds) **[2]**. This approach helped record extraordinary cylindrical shapes on vesicles **[3]**. These unusual morphologies (cylinders or disks with spherical caps) have not been previously observed due to their short lifetime of a few milliseconds. The observation with the fast digital camera allowed resolving the pores on the vesicle and the dynamics of the vesicle response **[2]**. The lifetime of the pores, which was in the millisecond range, was found to depend on the membrane viscosity. In the fluid phase, the latter can be determined from optical manipulation of a probe attached to the membrane (optical dynamometry) **[4]**. When the membrane undergoes a fluid-to-gel transition, the membrane viscosity drastically increases. Thus, it is to be expected that the lifetime of pores formed on vesicles in the gel phase would be much longer. We attempted to visualize such pores using confocal microscopy on giant vesicles in the gel phase; see **Fig. 3**. Indeed, the time of these pores to reseal was orders of magnitude longer than the lifetime of pores in electroporated membranes in the fluid phase **[5]**.

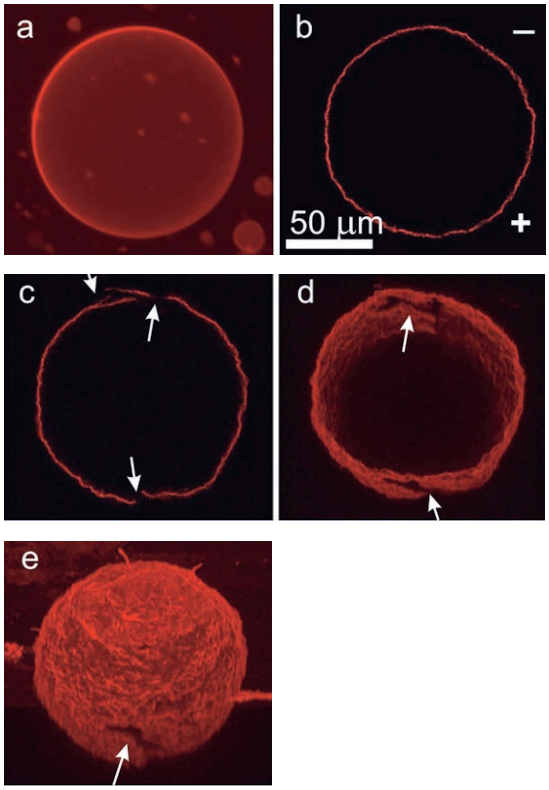

Fig. 3: Electroporation of a fluorescently labeled vesicle in the gel phase as imaged with confocal microscopy. (a) A 3d projection averaged image of a vesicle in the fluid phase. (b-e) Images of a vesicle in the gel phase: Equatorial sections of the vesicle before (b) and after poration (c) caused by an electric pulse of 300 V (6 KV/cm) and duration 300 microseconds. The electrode polarity is indicated with plus (+) and minus (-) signs in (b). The arrows in (c) show the ruptured zones at the vesicle poles. A 30 micrometer wide stripe from the equatorial area of the vesicle (slightly rotated around the horizontal axis) shows the ruptured places in the membrane at the north and south poles (d) as indicated with arrows. A complete 3d projection average image of the same vesicle (again rotated around the x-axis) shows better the crack on the southern pole of the vesicle (e) pointed by the arrow. Contrary to vesicles in the fluid phase (a), pores formed on vesicles in the gel phase (e) do not reseal over a period of at least ten minutes.

R. Dimova, S. Aranda, R. Knorr, K. A. Riske
Rumiana.Dimova@mpikg.mpg.de

References:

[1] Dimova, R., Aranda, S., Bezlyepkina, N., Nikolov, V., Riske, K. A. and Lipowsky, R.: A practical guide to giant vesicles. Probing the membrane nanoregime via optical microscopy. J. Phys.: Condens. Matter, **18**, S1151-S1176 (2006).
[2] Riske, K. A. and Dimova, R.: Electro-deformation and -poration of giant vesicles viewed with high temporal resolution. Biophys. J., **88**, 1143-1155 (2005).
[3] Riske, K. A. and Dimova, R.: Electric pulses induce cylindrical deformations on giant vesicles in salt solutions. Biophys. J. **91**, 1778-1786 (2006).
[4] Dimova, R. and Pouligny, B.: Optical dynamometry to study phase transitions in lipid membranes. in "Protocols in Biophysics to Study Membrane Lipids", ed. A. Dopico, Humana Press, in press.
[5] Dimova, R., Aranda, S., Riske, K. A., Knorr, R. and Lipowsky, R.: Vesicles in electric fields, in preparation.

Molecular Recognition in Membrane Adhesion

Thomas Weikl 01.04.1970
1996: Diploma, Physics
(Freie Universität Berlin)
Thesis: Interactions of rigid membrane inclusions
1999: PhD, Physics
(Max Planck Institute of Colloids and Interfaces, Potsdam)
Thesis: Adhesion of multicomponent membranes
2000-2002: Postdoc
(University of California, San Francisco)
Since 2002: Group Leader
(Max Planck Institute of Colloids and Interfaces, Potsdam)

Cells adhere to other cells via adhesion molecules located on their membrane surfaces. Each adhesion molecule on one cell binds to a "partner molecule" on the other cell. The two binding partners can be identical molecules, like two hands holding each other, or distinct molecules that fit together like a lock and a key. Cadherins, for example, are adhesion molecules that often bind to identical cadherins, holding together cells of the same type in the development and maintenance of body tissues. Integrins and selectins, on the other hand, bind to distinct adhesion partners, for example during adhesion of white blood cells in an immune defense.

The adhesion of two cells involves a subtle balance between the attractive binding energies of the adhesion molecules and repulsive energies, which result from cell shape fluctuations or from large non-adhesive proteins that impede adhesion. In a healthy organism, cells have to control this balance between attraction and repulsion. For some cancers, mutations of adhesion molecules shift the balance and lead to abnormal cell-cell adhesion events and tumor growth.

Active Switching of Adhesion Molecules

Via gene expression, cells can regulate the numbers and types of adhesion molecules at their surfaces and, thus, the strength and specifity of their adhesiveness. But some cells are known to change their adhesiveness rather quickly, much more quickly than gene expression allows. These cells have adhesion molecules that can be switched between different states. Integrins, for example, are adhesion molecules that have at least two different conformational states. In a "stretched" conformational state, the integrins are active and can bind to their partners on an apposing cell surface. In a "bent" state, the integrins are inactive and can't bind (see **Fig. 1**).

The numbers of active integrins are crucial for the adhesiveness of these cells. But besides mere numbers, other effects may count as well. We have shown that the characteristic switching rates of adhesion molecules can strongly affect the adhesiveness. The switching of an adhesion molecule between an active and an inactive conformation is a stochastic process, i.e. a process that occurs with a certain probability at a certain time. The process typically requires the input of "chemical energy", e.g., from ATP molecules, at least in one direction.

We have thus studied the adhesion of membranes via switchable adhesion molecules **[1, 2, 3]**. The two opposing forces in the adhesion balance of the membranes are the attractive forces of the adhesion molecules, and repulsive forces from membrane shape fluctuations. Both forces have characteristic times scales. These time scales are the switching times of the adhesion molecules, and the relaxation times of the membrane shape fluctuations. A resonance effect occurs if the characteristic times are similar (see **Fig. 1**). The resonance leads to an increase in membrane fluctuations, and to a decrease of the adhesiveness of the membranes **[1, 3]**.

This resonance effect may also be used to control cell adhesion. During the last decade, synthetic molecules have been developed that can be switched by light between different conformations. The switching times of such molecules depend on the light intensity. Anchored at a substrate, the molecules can be used to switch the adhesive substrate properties and, thus, to manipulate and study cell adhesion.

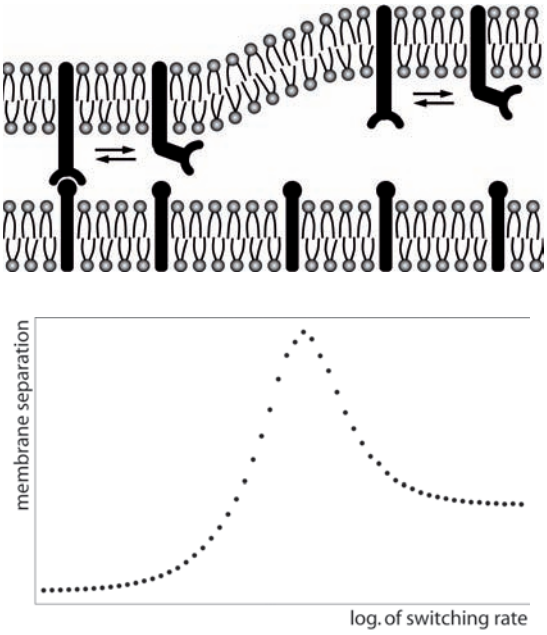

Fig. 1: (Top) A membrane with switchable adhesion molecules adhering to a second membrane. The adhesion molecules are switched between a stretched, active conformation and a bent, inactive conformation. In the stretched conformation, the adhesion molecules can bind to their ligands in the other membrane. (Bottom) Membrane separation as a function of the receptor switching rate. The active switching leads to a stochastic resonance with increased membrane separations at intermediate switching rates.

Long and Short Adhesion Molecules

The adhesion of biological membranes often involves various types of adhesion molecules. These adhesion molecules can have different lengths. The adhesion molecule complexes that mediate the adhesion of T cells, for example, have characteristic lengths of 15 or 40 nm. During T cell adhesion, a lateral phase separation into domains that are either rich in short or long adhesion molecules occurs. The domain formation is presumably caused by the length mismatch of the adhesion molecules **[4]**. The domains may play a central role for T cell signaling in immune responses.

We have developed a statistical-mechanical model for membranes interacting via various types of adhesion molecules **[4, 5]**. In our model, the membranes are discretized into small patches that can contain single adhesion molecules. The conformations of the membranes are characterized by the local separation of apposing membrane patches, and by the distribution of adhesion molecules in the membranes.

The equilibrium phase behavior of the membranes can be derived from the partition function of our model. The partition function is the sum over all possible membrane conformations, weighted by their Boltzmann factors. In our model, the summation over all possible distributions of the adhesion molecules in the partition function leads to an effective double-well potential (see **Fig. 2**). The depths of the wells depend on the concentrations and binding energies of the molecules.

The membranes exhibit two characteristic phase transitions. The first transition is the unbinding transition of the membranes, which is driven by an entropic membrane repulsion arising from thermal shape fluctuations. The second transition is lateral phase separation within the membranes, driven by the length mismatch of the adhesion molecules. The length mismatch leads to a membrane-mediated repulsion between long and short adhesion molecules, because the membranes have to be bent to compensate this mismatch, which costs elastic energy. This repulsion leads to a lateral phase separation for sufficiently large concentrations of the molecules and, thus, sufficiently deep wells of the effective potential (see **Fig. 3**).

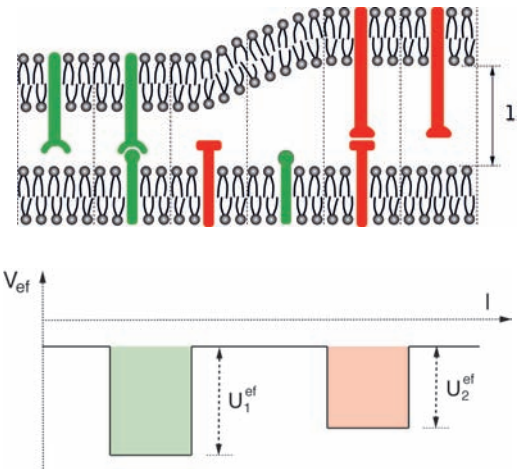

Fig. 2: (Top) A membrane containing long and short receptor molecules (upper membrane) adhering to a membrane with complementary ligands. (Bottom) The effective adhesion potential V_{ef} of the membranes is a double-well potential. The potential well at short separations l reflects the interactions of the short receptor/ligand bonds, the well at larger separations reflects the interactions of the long receptor/ligand bonds.

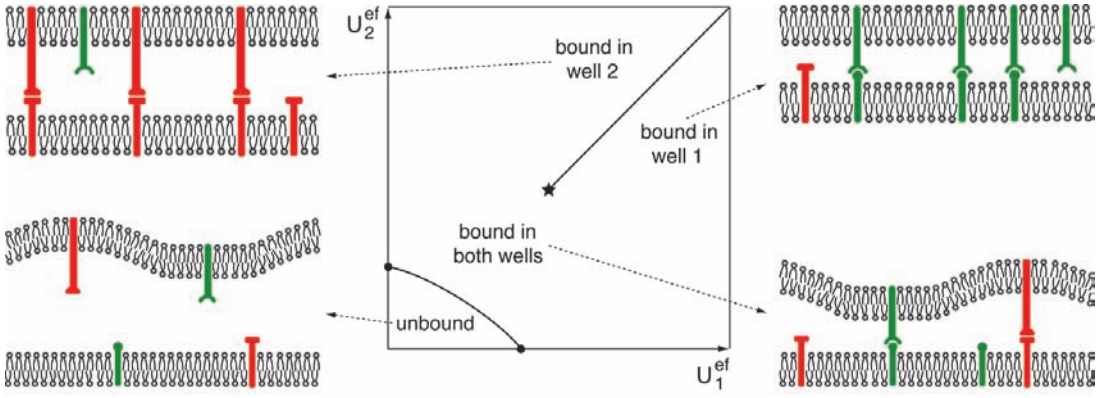

Fig. 3: Phase diagram of membranes adhering via long and short adhesion molecules. The membranes are unbound for small well depths U_1^{ef} and U_2^{ef} of the effective interaction potential shown in Fig. 2, i.e. for small concentrations or binding energies of receptors and ligands. At large values of U_1^{ef} and U_2^{ef}, the membranes are either bound in well 1 or well 2. At intermediate well depths, the membranes are bound in both potential wells.

T. Weikl, M. Asfaw, H. Krobath, B. Rozycki, R. Lipowsky
thomas.weikl@mpikg.mpg.de

References:

[1] Rozycki, B., Lipowsky, R., and Weikl, T. R.: Adhesion of membranes with active stickers. Phys. Rev. Lett. **96**, 048101 (2006).

[2] Rozycki, B., Weikl, T. R, and Lipowsky, R.: Adhesion of membranes via switchable molecules. Phys. Rev. E. **73**, 061908 (2006).

[3] Rozycki, B., Weikl, T. R, and Lipowsky, R.: Stochastic resonance for adhesion of membranes with active stickers. Eur. Phys. J. E, in press.

[4] Weikl, T. R., and Lipowsky, R.: Pattern formation during T cell adhesion. Biophys. J. **87**, 3665-3678 (2004).

[5] Asfaw, M., Rozycki, B., Lipowsky, R., and Weikl, T. R.: Membrane adhesion via competing receptor/ligand bonds. Europhys. Lett. **76**, 703-709 (2006).

Activity Patterns on Scale-Free Networks

Reinhard Lipowsky 11.11.1953
1978: Diploma, Physics,
Thesis with Heinz Horner on
turbulence (University of Heidelberg)
1982: PhD (Dr. rer. nat.), Physics
(University of Munich)
Thesis with Herbert Wagner
on surface phase transitions
1979-1984: Teaching Associate with
Herbert Wagner (University of Munich)
1984-1986: Research Associate with
Michael E. Fisher (Cornell University)
1986-1988: Research Associate with
Heiner Müller-Krumbhaar (FZ Jülich)
1987: Habilitation, Theoretical Physics
(University of Munich)
Thesis: Critical behavior of interfaces:
Wetting, surface melting and related
phenomena
1989-1990: Associate Professorship
(University of Munich)
1990-1993: Full Professorship
(University of Cologne), Director of
the Division "Theory II" (FZ Jülich)
Since Nov 1993: Director
(Max Planck Institute of Colloids
and Interfaces, Potsdam)

The biosphere contains many complex networks built up from rather different elements such as molecules, cells, organisms, or machines. In spite of their diversity, these networks exhibit some univeral features and generic properties. The basic elements of each network can be represented by nodes or vertices. Furthermore, any binary relation between these elements can be described by connections or edges between these vertices as shown in **Fig. 1**. By definition, the degree k of a given vertex is equal to the number of edges connected to it, i.e., to the number of direct neighbors. Large networks containing many vertices can then be characterized by their degree distribution, P(k), which represents the probability that a randomly chosen vertex has degree k.

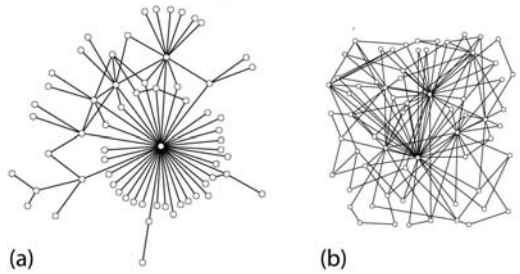

Fig. 1: Two examples for small scale-free networks: (a) Network with scaling exponent $\gamma = 2$ and minimal degree $k_0 = 1$. This network has a tree-like structure and a small number of closed cycles; and (b) Network with scaling exponent $\gamma = 5/2$ and minimal degree $k_0 = 2$ for which all edges belong to closed cycles.

Scale-Free Degree Distributions

Many biological, social, and technological networks are found to be scale-free in the sense that their degree distribution decays as

$$P(k) \sim 1/k^{\gamma} \text{ for } k > k_0$$

which defines the scaling exponent γ. Typical values for this exponent are found to lie between 2 and 5/2. **[1,2]** As one would expect naively, there are fewer vertices with a larger number of connections. However, since the probability P(k) decreases rather slowly with k, a large network with many vertices always contains some high-degree vertices with a large number of direct neighbors.

As an example, let us consider neural networks. The human brain consists of about 100 billion nerve cells or neurons that are interconnected to form a huge network. Each neuron can be active by producing an action potential. If we were able to make a snapshot of the whole neural network, we would see, at any moment in time, a certain pattern of active and inactive neurons. If we combined many such snapshots into a movie, we would find that this activity pattern changes continuously with time. At present, one cannot observe such activity patterns on the level of single neurons, but modern imaging techniques enable us to monitor coarse-grained patterns with a reduced spatial resolution. Using functional magnetic resonance imaging, for example, we can obtain activity patterns of about 100 000 neural domains, each of which contains about a million neurons.

These neural domains form another, coarse-grained network. Each domain corresponds to a vertex of this network, and each vertex can again be characterized by its degree k, i.e., by the number of connections to other vertices. It has been recently concluded from magnetic resonance images that the functional networks of neural domains are scale-free and characterized by a degree distribution with scaling exponent $\gamma = 2.1$.

Dynamical Variables and Activity Patterns

In general, the elements of real networks are dynamic and exhibit various properties that change with time. A more detailed description of the network is then obtained in terms of dynamical variables associated with each vertex of the network. In many cases, these variables evolve fast compared to changes in the network topology, which is therefore taken to be time-independent. Two examples for such dynamical processes are provided by neural networks that can be characterized by firing and nonfiring neurons or by the regulation of genetic networks that exhibit a changing pattern of active and inactive genes. In these examples, each dynamical variable can attain only two states (active or inactive), and the configuration of all of these variables defines the activity pattern of the network as shown in **Fig. 2**.

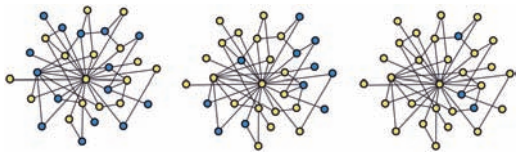

Fig. 2: Three subsequent snapshots of the activity pattern on a small scale-free network with 31 vertices and 50 edges. The active and inactive vertices are yellow and blue, respectively. For the initial pattern on the left, about half of the vertices are inactive (blue); for the final pattern on the right, almost all vertices are active (yellow). Each vertex of the network has a certain degree which is equal to the number of connections attached to it; this number is explicitly given for some nodes on the left.

Local Majority Rules Dynamics

In collaboration with Haijun Zhou (now professor at ITP, CAS, Beijing), we have recently started to theoretically study the time evolution of such activity patterns. **[3,4]** We focused on the presumably simplest dynamics as generated by a local majority rule: If, at a certain time, most direct neighbors of a certain vertex are active or inactive, this vertex will become active or inactive at the next update of the pattern. This dynamical rule leads to two fixed points corresponding to two completely ordered patterns, the all-active pattern and the all-inactive one. Each fixed point has a basin of attraction consisting of all patterns that evolve towards this fixed point for sufficiently long times. The boundary between the two basins of attraction of the two fixed points represents the so-called separatrix. One global characterization of the space of activity patterns is the distance of a fixed point from the separatrix as measured by the smallest number of vertices one has to switch from active to inactive (or vice versa) in order to reach the basin of attraction of the other fixed point.

Distance Between Fixed Points and Separatrix

We found that, for scale-free networks, this distance corresponds to selective switches of the high-degree vertices and strongly depends on the scaling exponent γ. For a network with N vertices, the number Ω of highly connected vertices that one has to switch in the all-active (or all-inactive) pattern in order to perturb this pattern beyond the separatrix grows as $\Omega = N/2^{\zeta}$ with $\zeta = (\gamma-1)/(\gamma-2)$ and vanishes as an essential singularity when the scaling exponent γ approaches the value $\gamma = 2$ from above. **[3]** If we used random rather than selective switches, on the other hand, we would have to switch of the order of N/2 vertices irrespective of the value of γ. Note that, in the limit in which the scaling exponent γ becomes large, selective and random switching lead to the same distance Ω. A low-dimensional cartoon of the high-dimensional pattern space is shown in **Fig. 3**.

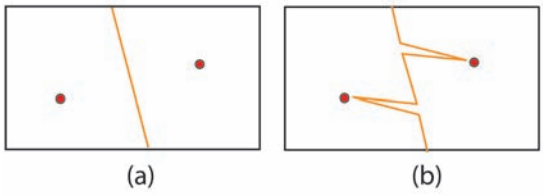

Fig. 3: Two fixed points (red dots) and separatrix (orange line) between their basins of attraction; (a) For large values of the scaling exponent γ the separatrix is smooth; (b) As the scaling exponent is decreased towards the value $\gamma = 2$, the separatrix develops spikes which come very close to the fixed points. These spikes correspond to the selective switching of the high-degree vertices.

Decay Times of Disordered Patterns

Another surprising feature of activity patterns on scale-free networks is the evolution of strongly disordered patterns that are initially close to the separatrix. These patterns decay towards one of the two ordered patterns but the corresponding decay time, i.e., the time it takes to reach these fixed points, again depends strongly on the scaling exponent γ.

We have developed a mean field theory that predicts qualitatively different behavior for $\gamma < 5/2$ and $\gamma > 5/2$. **[3,4]** For $2 < \gamma < 5/2$, strongly disordered patterns decay within a finite decay time even in the limit of infinite networks. For $\gamma > 5/2$, on the other hand, this decay time diverges logarithmically with the network size N. These mean field predictions have been checked by extensive computer simulations of two different ensembles of random scale-free networks using both parallel (or synchronous) as well as random sequential (or asynchronous) updating. **[4]** The two ensembles consist of (i) multi-networks that typically contain many self-connections and multiple edges and (ii) simple-networks without self-connections and multiple edges. For simple-networks, the simulations confirm the mean field results, see **Fig. 4**. For multi-networks, it is more difficult to determine the asymptotic behavior for large number of vertices since these networks are governed by an effective, N-dependent scaling exponent γ_{eff} that exceeds γ for finite values of N. **[4]**

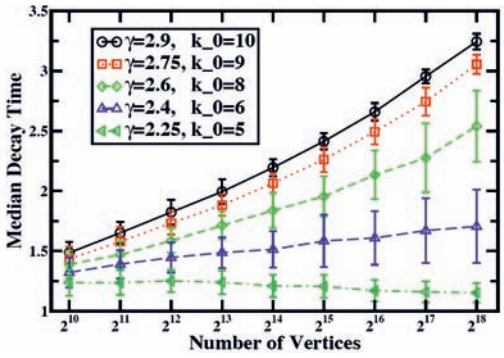

Fig. 4: Decay times for strongly disorderd patterns as a function of the number, N, of vertices contained in simple-networks for random sequential updating. The minimal vertex degree k_0 was chosen in such a way that the average degree is roughly equal for all values of the scaling exponent γ. In the limit of large N, the decay times attain a finite value for $\gamma < 5/2$ but increase logarithmically with N for $\gamma > 5/2$.

R. Lipowsky, J. Menche, A. Valleriani
reinhard.lipowsky@mpikg.mpg

References:

[1] Albert, R. and Barabasi, A.-L.: Statistical mechanics of complex networks. Rev. Mod. Phys. **74**, 47 (2002).
[2] Newman, M. E. J.: The structure and function of complex networks. SIAM Review **45**, 167 (2003).
[3] Zhou, H., and Lipowsky, R.: Dynamic pattern evolution on scale-free networks. PNAS **102**, 10052 (2005).
[4] Zhou, H., and Lipowsky, R.: Activity patterns on random scale-free networks: Global dynamics arising from local majority rules. J. Stat. Mech: Theory and Experiment **2007**, 01009 (2007).

Stochastic Modeling in Ecology and Evolution

Angelo Valleriani 14.03.1966
1992: Diploma, Physics (University of Bologna)
Thesis: Conformal Invariance, Renormalization Group and Integrable Models in Two-Dimensional Quantum Field Theories
1996: PhD, High-Energy Physics (SISSA-ISAS, Triest)
Thesis: Form Factors and Correlation Functions
1996-1998: Postdoc (Max Planck Institute for the Physics of Complex Systems, Dresden)
1998-2000: Postdoc (Max Planck Institute of Colloids and Interfaces, Potsdam)
Since 2000: Group Leader and IMPRS Coordinator (Max Planck Institute of Colloids and Interfaces, Potsdam)

Most environments in which life evolves have a stochastic nature. For a single natural population a particularly important element of stochasticity is produced by variations over time of the resources necessary for growth and reproduction. Another source of variation comes from the emergence of mutations that can spread in the population and change its structure in a stochastic manner. If we consider a group of species organized in a food web, the arrival of a new species (e.g. through immigration) or the local extinction of another species change the topology of the food web in an unpredictable manner.

Evolution of Dormancy

An interesting example of how natural populations cope with variations in time of the resources is provided by organisms leaving in extreme seasonal environments, where the conditions for growth and reproduction vary strongly from season to season. A much studied case of this kind is given by plants in deserts. In this environment, most plants are restricted to live only a few months during winter and the yield, i.e. the number of seeds produced by each plant, can strongly vary from season to season. Sometimes, even zero yields can occur. To adapt to such an environment, these species have developed two mechanisms. On the one hand, at the end of the season, the individuals devote all their energy to the production of their seeds and die afterwards. For this reason, they are called annual species. On the other hand, at the beginning of each of the next seasons the seeds will germinate only with a certain probability $g<1$ even if the conditions for germination are optimal. These seeds are then called dormant. Thus, dormancy is a strategy that maintains a permanent soil seed bank, which allows local populations to avoid extinction after seasons without yield **[1]**.

One important topic of theoretical population biology is to characterize the phenotypes that we would expect on the basis of evolution. In the case of dormant seeds, the phenotype is the fraction g of seeds in the seed bank that should germinate at the beginning of each season.

If the plants cannot predict how good or bad a season will be, they have two simple choices: all seeds germinate, i.e. $g=1$; or all seeds stay dormant, i.e. $g=0$. These two choices are called pure strategies in game theory. To find out whether evolution leads to one of the two pure strategies or to a mixed strategy, i.e. to $0<g<1$, one implements a method called invasibility analysis: we determine whether a small population playing the strategy g' can invade an environment dominated by a larger population playing the strategy g. By means of both analytical and numerical techniques **[2]**, this method allows to compute the strategy g^* which survives attempts of invasion by any other strategy. The strategy g^* is then called the evolutionarily stable strategy of the system. This means that evolution should lead to the phenotype g^*.

The analysis of how the evolutionarily stable strategy g^* depends on other parameters, provides important information about the effect of these parameters on the evolutionary history of the species. In the case of seed dormancy, such parameters are given by the statistical properties of the yield per season.

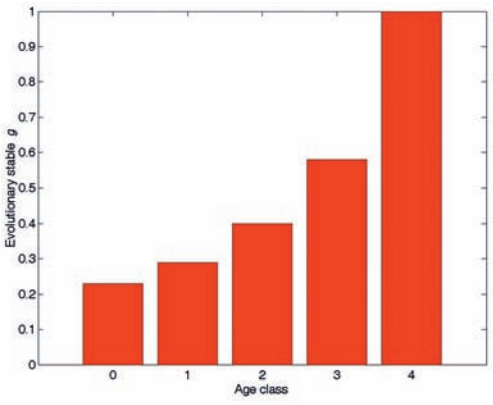

Fig. 1: The evolutionarily stable strategy for structured seed banks is that older seeds (right) have higher germination probability than younger seeds (left).

A particular issue that interested us was the analysis of the evolutionarily stable strategy when the seed bank is structured. One obvious reason for why the seed bank is structured is that there are seeds of several ages in the soil. If we consider each age as a class, then the seed bank is structured in age classes. From empirical studies on seeds, we know that several mechanical and biochemical processes have an effect on the germination properties of the seeds. We also know that these effects depend on time and therefore on age. This leads to the expectation that old viable seeds will react differently than younger seeds to optimal germination conditions but no theory existed to investigate this point. We have therefore developed and studied an evolutionary model to follow the evolution of g with the age of the seeds. The main result of the model is that the age-dependent g^* will grow with the age of the seeds (**Fig. 1**). This result is in agreement with the intuitive expectation. It tells also that there must be an adaptation to the mechanical and biochemical mechanisms which influence the germination behavior **[3]**.

Another, less obvious seed bank structure became clear from several empirical studies. It was noticed that several plant species in distinct locations produce seeds, which have a low germination probability after a large yield season, and seeds with a large germination probability after a low yield season (**Fig. 2**).

We have developed a different evolutionary model where we made the simplifying assumption that there are only two kinds

of seasons, good and bad ones. In this way, we could structure the seed bank into two classes: seeds from good seasons and seeds from bad seasons. Our analysis shows that it is evolutionary convenient that seeds from good seasons have a lower germination probability than those from bad seasons **[4]**.

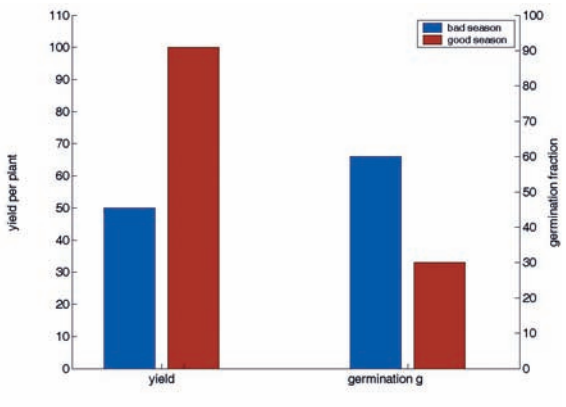

Fig. 2: Seeds from a bad season (blue) have a larger germination probability than seeds from a good season (red).

Given the very general assumptions of the model, we concluded that this behavior should be common to all annual species with permanent soil seed banks.

Often, empirical work aimed at measuring germination behavior is done by collecting and comparing seeds from different geographic locations, which show differences in the year-to-year time correlation of the environmental variables. These correlations, which have been discovered to be very common, are particular important in systems whose adaptive behavior depends on the degree of unpredictability of the quality of a given season. Since the theory so far could not take into account this effect in modeling seed dormancy, I have thus developed a model for the adaptive dynamics of dormancy with which the correlation in the yield are taken into account **[5]**. The result is that positive correlations soften the effect of stochasticity and thus enhance germination, while negative correlation work in the opposite direction.

The Structure of Ecological Networks

For a long time, ecologists are looking for explanations for the amount of biodiversity found in natural systems. It is in fact easy to show why biodiversity should be limited but it proved to be non-trivial to show under which conditions biodiversity can be large. In a sequence of two papers **[6, 7]** we took up this question and compared several mechanistic models using both mean field analysis and computer simulations.

Independently of the details of the mechanistic models, we found a relationship between the ecological characteristics of each species, which we called productivity, and the number of species that can coexist in a food web. Indeed, we have found that the variance of the productivities in a whole food web must decrease at least like 1/S in order to accommodate S species in the network **[6]**. Moreover, by simulating an ecological network in steady state under non equilibrium conditions of immigration and extinction, we could show that biodiversity increases as a power law of the immigration rate, in agreement with the empirical observations **[7]**.

When populations are split into groups connected by a migration network, the fate of mutants willing to spread into the whole population may depend on the structure of the network. By considering the simple Moran process for the population dynamics within each group and within the population, we have shown that a network with a preferred migration direction works against natural selection. This means that the probability of fixation of a favorable mutant is smaller than the probability of fixation in a non-structured or homogeneous network **[8]**.

Angelo Valleriani,
Angelo.Valleriani@mpikg.mpg.de

References:

[1] Bulmer, M.G. "Delayed Germination of Seeds: Cohen's Model Revisited". Theoretical Population Biology **26**, 367-377 (1984).
[2] Valleriani, A.: "Algebraic Determination of the Evolutionary Stable Germination Fraction". Theoretical Population Biology **68**, 197-203 (2005).
[3] Valleriani, A. and Tielbörger, K.: "Effect of Age on Germination of Dormant Seeds", Theoretical Population Biology **70**, 1-9 (2006).
[4] Tielbörger, K. and Valleriani, A.: "Can Seeds predict their Future? Germination Strategies of Density-Regulated Desert Annuals", OIKOS **111**, 235-244 (2005).
[5] Valleriani, A.: "Evolutionarily Stable Germination Strategies with Time-Correlated Yield", Theoretical Population Biology **70**, 255-271 (2006).
[6] Bastolla, U., Lässig, M., Manrubia, S.C. and Valleriani A.: "Biodiversity in Model Ecosystems, I: Coexistence Conditions for Competing Species", J. Theor. Biol. **235**, 521-530 (2005).
[7] Bastolla, U., Lässig, M., Manrubia, S.C. and Valleriani A.: "Biodiversity in Model Ecosystems, II: Species Assembly and Food Web Structure", J. Theor. Biol. **235**, 531-539 (2005).
[8] Valleriani, A. and Meene, T.: "Multilevel Selection in a Gradient", submitted to Ecological Modelling.

Holding with Invisible Light: Optical Trapping of Small and Large Colloidal Particles

Rumiana Dimova 06.04.1971
1995: Diploma, Chemistry (Sofia University, Bulgaria), Major: Chemical Physics and Theoretical Chemistry, Thesis: Role of the Ionic-Correlation and the Hydration Surface Forces in the Stability of Thin Liquid Films
1997: Second MSc (Sofia University, Bulgaria) Thesis: Interactions between Model Membranes and Micron-Sized Particles
1999: PhD, Physical Chemistry (Bordeaux University, France) Thesis: Hydrodynamical Properties of Model Membranes Studied by Means of Optical Trapping Manipulation of Micron-Sized Particles
2000: Postdoc (Max Planck Institute of Colloids and Interfaces, Potsdam)
Since 2001: Group Leader (Max Planck Institute of Colloids and Interfaces, Potsdam)

Early works on trapping and levitation of small objects by laser beams date back to the 1970s. Optical tweezers are now a widespread tool based on three-dimensional trapping by a single tightly focused laser beam (**Fig. 1a**). In general, the necessary condition for optical trapping of a particle is that the refractive index of the latter is higher than the one of the surrounding media. Due to the shape of the beam and the refraction from the surface of the particle, the bead is pushed towards the zone with higher intensity, i.e. the beam waist of the laser beam. Thus, using light one can manipulate particles without mechanically touching them. Even though they are difficult to work with because of being invisible for the human eye, infrared laser sources are preferred for the lower potential damage on biological samples.

The simplicity of laser tweezers stems from the fact that to construct a trap one just needs a single collimated beam, directed through a microscope objective with a very large aperture. The latter condition implies using short-working-distance objectives, which restrict optical manipulation to the high magnification end of the microscope nosepiece. Certain applications of optical trapping demand long-working distances at moderate magnification. This can be achieved using a two-beam trapping configuration where two counterpropagating laser beams are used (**Fig. 1b**).

Both single- and two-beam trappings have advantages and drawbacks. All of the limitations of the single-beam trap are consequences of the requirement of a very large aperture objective. (i) Such objectives are of immersion type and have extremely short-working distances: one is limited to working at distances not larger than about 10 μm above the chamber bottom. (ii) They are at the high magnification end (100x is standard) of the microscope nosepiece, providing a relatively narrow field of view. (iii) Large aperture means high resolution, which is profitable, but involves, at the same time, tight focusing and very high power density. The latter often causes heating and optical damage to the sample.

The two-beam geometry represents an opposite tradeoff. Beams are weakly focused by low aperture objectives, allowing for long working distances, low magnification and large field of view, and moderate intensities. Drawbacks are (i) a definitely higher complexity of the optical setup, which needs shaping, aligning, and precisely positioning a couple of counterpropagating beams; and (ii) the trapping geometry depends on the particle size.

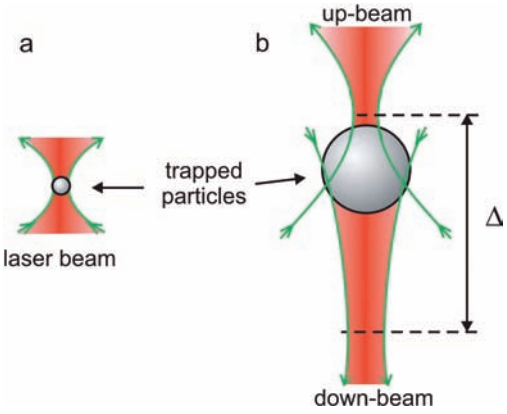

Fig. 1: A schematic illustration of single-beam (a) and double-beam optical trapping (b). In the first case, the laser beam is tightly focused by the objective and the particle is trapped at the beam waist position. In the case of a double-beam trap, two counterpropagating beams are used, up-going and down-going. Their beam waists are located above and below the bead, forming a trapping cage for the particle. The inter-focal distance Δ is set depending on the particle size.

The particle sizes, which one can trap with the two types of traps, also differ. The single-beam tweezers are usually applied to manipulation of particles with diameters between about 0.5 and 5 micrometers. The lower range is set by the limitation from the optical detection of the manipulated particle. Some enhanced detection systems (for example, quadrant photo diodes, which follow the beam deflection from the trapped particles) can reduce this limit. The upper range of particle sizes is set by the diameter of the beam waist, which, in turn is fixed and depends on the objective characteristics. Thus, particles much larger than the beam waist cannot be suitably trapped. With the two-beam trap, one can easily manipulate large particles of tens of microns in size. However, due to the objectives of low magnification, this configuration cannot be applied to particles smaller than about 2 micrometers.

While single-beam tweezers are commercially available, double-beam traps are found only as home-built setups. Being aware of the advantages of having both configurations, recently in our lab, we developed a complete setup, which combines single- and two-beam trapping **[1]**. Both functions were integrated into a commercial microscope (Zeiss Axiovert 200M), and are compatible with all observation modes of the microscope (phase contrast, differential interference contrast, fluorescent microscopy). The system is fed by a continuous wave

Nd:YAG laser with wavelength 1064 nm. We evaluated the performance of the setup in both trapping modes with latex particles, either fluorescent or not, of different sizes, in the 1–20 µm range. In addition, the trapping ability for manipulating oil droplets and polymer capsules (the latter were provided by the Interface department) was also tested; see **Fig. 2**. Both single-beam and double-beam configuration can be used in the case of capsule manipulation. Because the capsules are much larger than the beam waist, in the single-beam configuration the laser beam is focused on a point located at the shell of the capsule where the force is applied. With the double-beam trap, one can capture the complete capsule in the trapping cage.

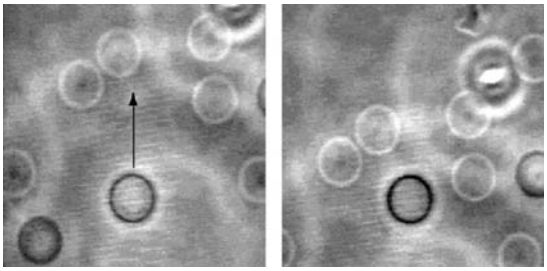

Fig. 2: Demonstration for trapping a polyelectrolyte capsule (phase contrast microscopy). In the setup, the laser beam is immobile and the sample stage is displaced. We trapped a single capsule, levitated it from the bottom of the observation chamber so that the rest of the capsules is out of focus (first snapshot) and displaced the sample stage. In this way, the particle was moved relative to the surrounding solution of capsules (compare with the background in the second snapshot). The direction of the relative displacement is indicated with an arrow in the first snapshot. The capsule diameter is approximately 6 micrometers.

Currently, the setup is used for the manipulation of micron beads with molecular motors attached to them (PhD project of Janina Beeg). The question we attempt to tackle concerns the collective transport of molecular motors. A considerable amount of studies have addressed the transport properties of single motor proteins. But the collective transport performed by several motors, as in the context of transport in cells, has not been studied in detail. As molecular motor we use kinesin, which walks on microtubule tracks. A micron-sized particle with certain kinesin coverage is trapped with the laser tweezers (single-beam mode) and brought to a selected microtubule; see **Fig. 3**. Only a certain fraction of the motors are involved in the bead displacement. The transport properties like walking distance, binding rate and escape force are characterized.

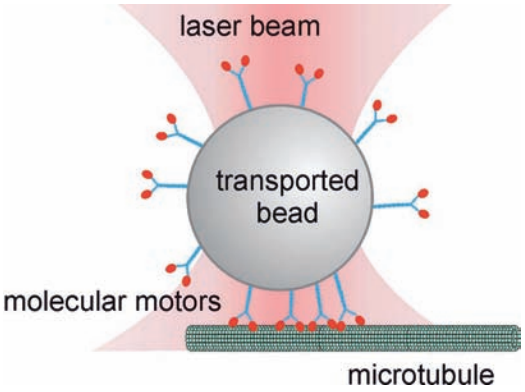

Fig. 3: A schematic illustration of the transport of a bead by several kinesin motors along a microtubule. The particle coverage with motors can be varied depending on the preparation conditions. The bead is trapped by optical tweezers and positioned at a microtubule. If released from the trap, it walks away being pulled by several motors. Switching on the trap again can apply a force in the picoNewton range which is enough to stop the processing bead.

R. Dimova, J. Beeg, P. Kraikivski
Rumiana.Dimova@mpikg.mpg.de

References:

[1] Kraikivski, P., Pouligny, B. and Dimova, R.: Implementing both short- and long-working-distance optical trapping into a commercial microscope, Rev. Sci. Instrum. **77**, 113703 (2006).

[2] Beeg, J., Klumpp, S., Dimova, R., Gracia, R. S., Unger, E. and Lipowsky, R.: Transport of beads by several kinesin motors, submitted.